

# Quark transverse charge densities in the $\Delta(1232)$ from lattice QCD

Constantia Alexandrou<sup>a</sup>, Tomasz Korzec<sup>a</sup>, Giannis Koutsou<sup>a</sup>, Cédric Lorcé<sup>b</sup>,  
John W. Negele<sup>c</sup>, Vladimir Pascalutsa<sup>b</sup>, Antonios Tsapalis<sup>d</sup>, Marc  
Vanderhaeghen<sup>b</sup>

<sup>a</sup>*Department of Physics, University of Cyprus, P.O. Box 20537, 1678 Nicosia, Cyprus*

<sup>b</sup>*Institut für Kernphysik, Johannes Gutenberg-Universität, D-55099 Mainz, Germany*

<sup>c</sup>*Center for Theoretical Physics, Laboratory for Nuclear Science and Department of Physics, Massachusetts Institute of Technology, Cambridge, Massachusetts 02139, U.S.A.*

<sup>d</sup>*Institute of Accelerating Systems and Applications, University of Athens, Athens, Greece*

---

## Abstract

We extend the formalism relating electromagnetic form factors to transverse quark charge densities in the light-front frame to the case of a spin-3/2 baryon and calculate these transverse densities for the  $\Delta(1232)$  isobar using lattice QCD. The transverse charge densities for a transversely polarized spin-3/2 particle are characterized by monopole, dipole, quadrupole, and octupole patterns representing the structure beyond that of a pure point-like spin-3/2 particle. We present lattice QCD results for the  $\Delta$ -isobar electromagnetic form factors for pion masses down to approximately 350 MeV for three cases: quenched QCD, two-degenerate flavors of dynamical Wilson quarks, and three flavors of quarks using a mixed action that combines domain wall valence quarks and dynamical staggered sea quarks. We extract transverse quark charge densities from these lattice results and find that the  $\Delta$  is prolately deformed, as indicated by the fact that the quadrupole moment  $G_{E2}(0)$  is larger than the value  $-3$  characterizing a point particle and the fact that the transverse charge density in a  $\Delta^+$  of maximal transverse spin projection is elongated along the axis of the spin.

*Key words:* Electromagnetic form factors, Electric and Magnetic Moments,  $\Delta$ -resonance

*PACS:* 13.40.Gp, 13.40.Em, 14.20.Gk

---

## 1. Introduction

The question of how the structure of mesons and baryons arises from the interaction among their quark and gluon constituents is at the forefront of contemporary research in hadron physics. Key observables in this field are the electromagnetic (e.m.) form factors (FFs), which yield the distribution of the quark charges in a hadron. The nucleon e.m. FFs have been especially thoroughly studied recently at electron-beam facilities, such as Jefferson Lab, MIT-Bates, and MAMI, see Refs. [1, 2, 3] for latest reviews.

In systems like nuclei or atoms, in which the spatial size  $R$  is large compared to the system's Compton wavelength  $1/M$ , electromagnetic form factors are essentially three dimensional Fourier transforms (or distorted wave analogs thereof) of ground state charge density distributions, and thereby provide valuable physical insight into the structure of the ground state of the system in the lab frame. In hadrons, however, where  $R \sim 1/M$ , the Fourier transform argument is inapplicable, and there is no known way to relate form factors to charge densities in the lab frame. However, when the hadron is viewed from a light front, there is a simple and consistent field-theoretic density interpretation of FFs as the Fourier transform of the spatial distribution of the quark charge in the plane transverse to the line-of-sight. Equivalently, in the infinite momentum frame, the quantity that plays the role of  $M$  in the lab frame Fourier transform argument is the light-front momentum  $p^+$ , which goes to infinity, so the form factor is just the two-dimensional Fourier transform of the transverse density in the infinite momentum frame [4]. In this way, the transverse quark charge densities have been mapped out in the nucleon [5, 6], deuteron [7], and pion [8] based on empirical FFs. It is important to note, however, that physics in the lab and infinite momentum frames is significantly different and hence there is no simple relation between the two-dimensional transverse densities in the infinite momentum (or light front) frame and the three-dimensional density in the lab frame, and we will return to this issue in the discussion of deformation.

In this work we address the e.m. FFs and transverse charge densities of the  $\Delta(1232)$  isobar, the lightest nucleon excitation. The nucleon-to- $\Delta$  transition has been well measured experimentally over a large range of photon virtualities, see Ref. [9] for a recent review. It is dominated by a magnetic dipole transition, while the electric and Coulomb quadrupole transitions were found to be small (in the few percent range as compared to the magnetic dipole transition). These measurements have made it possible to quantify the deformation of the  $N \rightarrow \Delta$  transition charge distribution [6].

On the other hand, the information on the e.m. FFs of the  $\Delta$  itself is scarce. Because of the tiny lifetime of the  $\Delta$ , it is of course very difficult if not impossible to access these quantities directly in experiment. Fortunately, however, as in the case of the  $N \rightarrow \Delta$  FFs, it is now feasible to calculate the  $\Delta$  FFs using lattice QCD. First lattice QCD results in the quenched approximation were presented in Ref. [10], and first results on the  $\Delta$  FFs using dynamical quarks were briefly reported in [11]. In this more extended publication we provide further details on the lattice evaluation of these FFs as well as the interpretation of the calculated FFs in terms of the transverse charge densities.

The outline of the paper is as follows: Section 2, contains a general discussion of the e.m. interaction of a spin-3/2 system along with the definition of its e.m. moments and FFs. In Section 3, we find the specific ('natural') values for electromagnetic moments that an elementary (pointlike) spin-3/2 particle would possess. In Section 4, we introduce the light-front helicity amplitudes for the e.m. vertex of a spin-3/2 system, and express them in terms of the corresponding e.m. FFs. In Section 5, we calculate quark transverse charge densities of a spin-3/2 system in terms of the light-front helicity amplitudes. We also calculate

the values of the electric dipole, quadrupole and octupole moments of these transverse charge densities, and show that for a pointlike spin-3/2 particle they vanish. In Section 6, we describe our three different types of lattice calculations of the  $\Delta(1232)$  e.m. FFs and compare their results. In the first type, we use Wilson fermions in the quenched approximation. The second type uses two-degenerate flavors of dynamical Wilson quarks ( $N_F = 2$ ). The third type uses a mixed action combining domain wall valence quarks with dynamical staggered sea quarks including light degenerate up and down quarks and heavier strange quarks ( $N_F = 2 + 1$ ). In Section 7, we use these lattice QCD results to extract the transverse quark charge densities in the  $\Delta$  resonance. We summarize our results, discuss their relation to models and present our conclusions in Section 8. The lattice results for the  $\Delta$  e.m. FFs are tabulated in an Appendix.

## 2. The $\gamma^* \Delta \Delta$ vertex and form factors

Let us consider the coupling of a photon to a  $\Delta$ , shown in Fig. 1. The matrix element of the electromagnetic current operator  $J^\mu$  between spin-3/2 states can be decomposed into four multipole transitions: a Coulomb monopole (E0), a magnetic dipole (M1), a Coulomb quadrupole (E2) and a magnetic octupole (M3). We first write a Lorentz-covariant decomposition for the on-shell  $\gamma^* \Delta \Delta$  vertex, which exhibits manifest electromagnetic gauge-invariance [9, 12]:

$$\begin{aligned} & \langle \Delta(p', \lambda') | J^\mu(0) | \Delta(p, \lambda) \rangle \\ &= -\bar{u}_\alpha(p', \lambda') \left\{ \left[ F_1^*(Q^2) g^{\alpha\beta} + F_3^*(Q^2) \frac{q^\alpha q^\beta}{(2M_\Delta)^2} \right] \gamma^\mu \right. \\ & \left. + \left[ F_2^*(Q^2) g^{\alpha\beta} + F_4^*(Q^2) \frac{q^\alpha q^\beta}{(2M_\Delta)^2} \right] \frac{i\sigma^{\mu\nu} q_\nu}{2M_\Delta} \right\} u_\beta(p, \lambda), \end{aligned} \quad (1)$$

where  $M_\Delta = 1.232$  GeV is the  $\Delta$  mass,  $u_\alpha$  is the Rarita-Schwinger spinor for a spin-3/2 state, and  $\lambda$  ( $\lambda'$ ) are the initial (final)  $\Delta$  helicities. Furthermore,  $F_{1,2,3,4}^*$  are the  $\gamma^* \Delta \Delta$  form factors, and  $F_1^*(0) = e_\Delta$  is the  $\Delta$  electric charge in units of  $e$  (e.g.,  $e_{\Delta^+} = +1$ ). For future reference, we also define the quantity  $\tau \equiv Q^2/(4M_\Delta^2)$ .

A physical interpretation of the four electromagnetic  $\Delta \rightarrow \Delta$  transitions can be obtained by performing a multipole decomposition [13, 12]. For this purpose it is convenient to consider the Breit frame, where  $\vec{p} = -\vec{p}' = -\vec{q}/2$ . Furthermore, we choose  $\vec{q}$  along the  $z$ -axis and denote the initial (final)  $\Delta$  spin projections along the  $z$ -axis by  $s$  ( $s'$ ). In this frame, the matrix elements of the charge operator define the Coulomb monopole (charge) and Coulomb quadrupole form factors as :

$$\begin{aligned} \langle \frac{\vec{q}}{2}, s' | J^0(0) | -\frac{\vec{q}}{2}, s \rangle & \equiv (2M_\Delta) \delta_{s's} \left\{ \left( \delta_{s \pm \frac{3}{2}} + \delta_{s \pm \frac{1}{2}} \right) G_{E0}(Q^2) \right. \\ & \left. - \frac{2}{3} \tau \left( \delta_{s \pm \frac{3}{2}} - \delta_{s \pm \frac{1}{2}} \right) G_{E2}(Q^2) \right\}. \end{aligned} \quad (2)$$

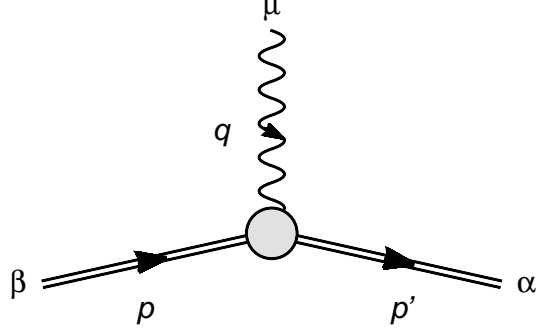


Figure 1: The  $\gamma^* \Delta \Delta$  vertex. The four-momenta of the initial (final)  $\Delta$  and of the photon are given by  $p$  ( $p'$ ) and  $q$  respectively. The four-vector indices of the initial (final) spin-3/2 fields are given by  $\beta$  ( $\alpha$ ), and  $\mu$  is the four-vector index of the photon field.

Using Eq. (1), we can express the Coulomb monopole and quadrupole form factors in terms of  $F_{1,2,3,4}^*$  as :

$$G_{E0} = (F_1^* - \tau F_2^*) + \frac{2}{3} \tau G_{E2}, \quad (3)$$

$$G_{E2} = (F_1^* - \tau F_2^*) - \frac{1}{2} (1 + \tau) (F_3^* - \tau F_4^*). \quad (4)$$

Analogously, the matrix elements of the current operator define the magnetic dipole and magnetic octupole form factors. For the transverse spherical component  $J_{+1} \equiv -\frac{1}{\sqrt{2}}(J^1 + iJ^2)$  we obtain :

$$\begin{aligned} \langle \frac{\vec{q}}{2}, s' | J_{+1}(0) | -\frac{\vec{q}}{2}, s \rangle &\equiv (-\sqrt{2})(2M_\Delta) \frac{\sqrt{\tau}}{\sqrt{3}} \\ &\times \left\{ \left( \delta_{s'+\frac{3}{2}} \delta_{s+\frac{1}{2}} + \delta_{s'-\frac{1}{2}} \delta_{s-\frac{3}{2}} + \frac{2}{\sqrt{3}} \delta_{s'+\frac{1}{2}} \delta_{s-\frac{1}{2}} \right) G_{M1}(Q^2) \right. \\ &\left. - \frac{4}{5} \tau \left( \delta_{s'+\frac{3}{2}} \delta_{s+\frac{1}{2}} + \delta_{s'-\frac{1}{2}} \delta_{s-\frac{3}{2}} - \sqrt{3} \delta_{s'+\frac{1}{2}} \delta_{s-\frac{1}{2}} \right) G_{M3}(Q^2) \right\} \quad (5) \end{aligned}$$

Using Eq. (1), we can express the magnetic dipole and octupole form factors in terms of  $F_{1,2,3,4}^*$  as :

$$G_{M1} = (F_1^* + F_2^*) + \frac{4}{5} \tau G_{M3}, \quad (6)$$

$$G_{M3} = (F_1^* + F_2^*) - \frac{1}{2} (1 + \tau) (F_3^* + F_4^*). \quad (7)$$

At  $Q^2 = 0$ , the multipole form factors define the charge ( $e_\Delta$ ), the magnetic dipole moment ( $\mu_\Delta$ ), the electric quadrupole moment ( $Q_\Delta$ ), and the magnetic

octupole moment ( $O_\Delta$ ) as :

$$e_\Delta = G_{E0}(0) = F_1^*(0), \quad (8a)$$

$$\mu_\Delta = \frac{e}{2M_\Delta} G_{M1}(0) = \frac{e}{2M_\Delta} [e_\Delta + F_2^*(0)], \quad (8b)$$

$$Q_\Delta = \frac{e}{M_\Delta^2} G_{E2}(0) = \frac{e}{M_\Delta^2} \left[ e_\Delta - \frac{1}{2} F_3^*(0) \right], \quad (8c)$$

$$O_\Delta = \frac{e}{2M_\Delta^3} G_{M3}(0) = \frac{e}{2M_\Delta^3} \left[ e_\Delta + F_2^*(0) - \frac{1}{2} (F_3^*(0) + F_4^*(0)) \right]. \quad (8d)$$

In the following, we will also use the relations that express the form factors  $F_{1,2,3,4}^*$  in terms of the multipole form factors :

$$\begin{aligned} F_1^* &= \frac{1}{1+\tau} \left\{ G_{E0} - \frac{2}{3}\tau G_{E2} + \tau \left[ G_{M1} - \frac{4}{5}\tau G_{M3} \right] \right\}, \\ F_2^* &= -\frac{1}{1+\tau} \left\{ G_{E0} - \frac{2}{3}\tau G_{E2} - \left[ G_{M1} - \frac{4}{5}\tau G_{M3} \right] \right\}, \\ F_3^* &= \frac{2}{(1+\tau)^2} \left\{ G_{E0} - \left( 1 + \frac{2}{3}\tau \right) G_{E2} + \tau \left[ G_{M1} - \left( 1 + \frac{4}{5}\tau \right) G_{M3} \right] \right\}, \\ F_4^* &= -\frac{2}{(1+\tau)^2} \left\{ G_{E0} - \left( 1 + \frac{2}{3}\tau \right) G_{E2} - \left[ G_{M1} - \left( 1 + \frac{4}{5}\tau \right) G_{M3} \right] \right\}. \end{aligned} \quad (9)$$

For completeness we also express the form factors in terms of the covariant vertex functions  $a_1, a_2, c_1$  and  $c_2$ , used for instance in references [12, 14, 11] :

$$F_1^* = a_1 + a_2, \quad F_2^* = -a_2, \quad F_3^* = c_1 + c_2, \quad F_4^* = -c_2. \quad (10)$$

These relations, together with the identity

$$\bar{u}_\alpha(p', \lambda') i\sigma^{\mu\nu} q_\nu u_\beta(p, \lambda) = \bar{u}_\alpha(p', \lambda') (2M_\Delta \gamma^\mu - [p + p']^\mu) u_\beta(p, \lambda) \quad (11)$$

bring Eq. (1) into the form introduced in [12, 14, 11].

The empirical knowledge of the  $\Delta$  electromagnetic moments is scarce, even though there were several attempts to measure the magnetic moment. The current Particle Data Group value of the  $\Delta^+$  magnetic dipole moment is given as [15]:

$$\mu_{\Delta^+} = 2.7_{-1.3}^{+1.0}(\text{stat.}) \pm 1.5(\text{syst.}) \pm 3(\text{theor.}) \mu_N, \quad (12)$$

where  $\mu_N = e/2M_N$  is the nuclear magneton. This result was obtained from *radiative photoproduction* ( $\gamma N \rightarrow \pi N \gamma'$ ) of neutral pions in the  $\Delta(1232)$  region by the TAPS Collaboration at MAMI [16], using a phenomenological model of the  $\gamma p \rightarrow \pi^0 p \gamma'$  reaction [17]. For the  $\Delta^+$ , Eq. (12) implies :

$$G_{M1}(0) = 3.5_{-1.7}^{+1.3}(\text{stat.}) \pm 2.0(\text{syst.}) \pm 3.9(\text{theor.}). \quad (13)$$

The size of the error-bar is rather large due to both experimental and theoretical uncertainties. Recently a dedicated experimental effort is underway at MAMI

using the Crystal Ball detector [18], aiming at improving on the statistics of the TAPS data by almost two orders of magnitude.

For the  $\Delta$  electric quadrupole moment, no direct measurements exist. However the electric quadrupole moment for the  $N \rightarrow \Delta$  transition has been measured accurately from the  $\gamma N \rightarrow \pi N$  reaction at the  $\Delta$  resonance energy [19] :

$$Q_{p \rightarrow \Delta^+} = -(0.0846 \pm 0.0033) \text{ e} \cdot \text{fm}^2. \quad (14)$$

In the large- $N_c$  limit of QCD, the two are related as follows [20]:

$$\frac{Q_{\Delta^+}}{Q_{p \rightarrow \Delta^+}} = \frac{2\sqrt{2}}{5} + \mathcal{O}\left(\frac{1}{N_c^2}\right), \quad (15)$$

which, using the empirical value for  $Q_{p \rightarrow \Delta^+}$  yields for the  $\Delta^+$  quadrupole moment:

$$Q_{\Delta^+} = -(0.048 \pm 0.002) \text{ e} \cdot \text{fm}^2, \quad (16)$$

accurate up to corrections of order  $1/N_c^2$ . Note that using Eq. (8d), the value in Eq. (16) implies  $G_{E2}(0) = -1.87 \pm 0.08$ .

### 3. The ‘natural’ values of the e.m. moments

As first argued by Weinberg [21], based on the Gerasimov-Drell-Hearn sum rule, there is a ‘natural’ value for the magnetic moment of a pointlike particle with spin, which corresponds to a gyromagnetic ratio  $g$  equal to 2. It has later been observed that all consistent field theories of charged particles with spin respect this value, see e.g. [22, 23]. Given this universal result for the magnetic moment, it is reasonable to expect that all electromagnetic moments of pointlike particles are fixed at ‘natural’ values. To determine the values for the spin-3/2 case, we examine the values of the e.m. moments of the gravitino in extended supergravity [24, 25].

The gravitino, if it existed, would be a spin-3/2 particle described by a Rarita-Schwinger field which, in the framework of  $\mathcal{N} = 2$  supergravity, couples consistently to electromagnetism. We therefore expect that all the e.m. moments arising in this theory are ‘natural’. To find their values, we start from the following Lagrangian density:<sup>1</sup>

$$\begin{aligned} \mathcal{L} &= \bar{\psi}_\mu \gamma^{\mu\nu\alpha} (i\partial_\alpha - eA_\alpha) \psi_\nu - m \bar{\psi}_\mu \gamma^{\mu\nu} \psi_\nu \\ &+ em^{-1} \bar{\psi}_\mu (i\kappa_1 F^{\mu\nu} - \kappa_2 \gamma_5 \tilde{F}^{\mu\nu}) \psi_\nu. \end{aligned} \quad (17)$$

It describes the spin-3/2 Rarita-Schwinger field ( $\psi_\mu$ ) with mass  $m$  coupled to the electromagnetic field ( $A_\mu$ ) via the minimal coupling (with positive charge

---

<sup>1</sup>In our conventions:  $\gamma^{\mu\nu} = \frac{1}{2}[\gamma^\mu, \gamma^\nu]$ ,  $\gamma^{\mu\nu\alpha} = \frac{1}{2}\{\gamma^{\mu\nu}, \gamma^\alpha\}$ ,  $F^{\mu\nu} = \partial^\mu A^\nu - \partial^\nu A^\mu$ ,  $\tilde{F}^{\mu\nu} = \varepsilon^{\mu\nu\rho\lambda} \partial_\rho A_\lambda$ .

e) and two non-minimal couplings  $\kappa_1$  and  $\kappa_2$ . As shown in Ref. [26], this is the most general Lagrangian of this type that gives the right number of spin degrees of freedom for a spin-3/2 particle. This theory, however, would still lead to rather subtle pathologies such as non-causal wave propagation [27, 28], at least if no other fields are present. Adding gravity in a supersymmetric way makes the theory fully consistent from this viewpoint, but also constrains the non-minimal couplings as follows:

$$\kappa_1 = \kappa_2 = 1. \quad (18)$$

We shall refer to these values as the ‘SUGRA choice’.

The e.m. vertex stemming from Eq. (17) is

$$\Gamma^{\alpha\beta\mu}(p', p) = \gamma^{\alpha\beta\mu} - \frac{\kappa_1}{m}(q^\alpha g^{\beta\mu} - q^\beta g^{\alpha\mu}) + i\frac{\kappa_2}{m}\gamma_5 \varepsilon^{\alpha\beta\mu\varrho} q_\varrho, \quad (19)$$

where  $q = p' - p$ , and  $\varepsilon_{0123} = +1$ . It is easy to verify that this coupling conserves the e.m. current:

$$q_\mu \bar{u}_\alpha(p') \Gamma^{\alpha\beta\mu}(p', p) u_\beta(p) = 0, \quad (20)$$

as well as, for the SUGRA choice, the supersymmetric current:

$$(p'_\alpha - \frac{1}{2}m\gamma_\alpha) \Gamma^{\alpha\beta\mu}(p', p) u_\beta(p) \epsilon_\mu(q) = 0, \quad (21a)$$

$$\bar{u}_\alpha(p') \Gamma^{\alpha\beta\mu}(p', p) (p_\beta - \frac{1}{2}m\gamma_\beta) \epsilon_\mu(q) = 0, \quad (21b)$$

where  $\epsilon_\mu(q)$  is the photon polarization vector, and  $q \cdot \epsilon = 0 = q^2$  in Eqs. (21).

The matrix elements of this vertex can be compared with the general decomposition of the spin-3/2 e.m. current given in Eq. (1), and in doing so we obtain the following result:

$$F_1^* = 1 + 2(\kappa_1 + \kappa_2) \tau \stackrel{\text{sugra}}{=} 1 + 4\tau, \quad (22a)$$

$$F_2^* = 2\kappa_1 \stackrel{\text{sugra}}{=} 2, \quad (22b)$$

$$F_3^* = 4(\kappa_1 + \kappa_2) \stackrel{\text{sugra}}{=} 8, \quad (22c)$$

$$F_4^* = 0, \quad (22d)$$

Thus, the values of gravitino’s e.m. moments in  $\mathcal{N} = 2$  supergravity are:

$$G_{E0}(0) = 1, \quad G_{M1}(0) = 3, \quad G_{E2}(0) = -3, \quad G_{M3}(0) = -1. \quad (23)$$

We take these values as the ‘natural’ values characterizing a structureless spin-3/2 particle, and interpret any deviation from them as a signature of internal structure.

#### 4. The $\gamma^* \Delta \Delta$ light-front helicity amplitudes

In the following, we consider the electromagnetic  $\Delta \rightarrow \Delta$  transition when viewed from a light front moving towards the  $\Delta$ . Equivalently, this corresponds

to a frame where the baryons have a large momentum-component along the  $z$ -axis chosen along the direction of  $P = (p + p')/2$ , where  $p$  ( $p'$ ) are the initial (final) baryon four-momenta. We indicate the baryon light-front + component by  $P^+$  (defining  $a^\pm \equiv a^0 \pm a^3$ ). We can furthermore choose a symmetric frame where the virtual photon four-momentum  $q$  has  $q^+ = 0$ , and has a transverse component (lying in the  $xy$ -plane) indicated by the transverse vector  $\vec{q}_\perp$ , satisfying  $q^2 = -\vec{q}_\perp^2 \equiv -Q^2$ . In such a symmetric frame, the virtual photon only couples to forward moving partons and the + component of the electromagnetic current  $J^+$  has the interpretation of the quark charge density operator. It is given by :  $J^+(0) = +2/3 \bar{u}(0)\gamma^+u(0) - 1/3 \bar{d}(0)\gamma^+d(0)$ , considering only  $u$  and  $d$  quarks. Each term in the expression is a positive operator since  $\bar{q}\gamma^+q \propto |\gamma^+q|^2$ .

We start by expressing the matrix elements of the  $J^+(0)$  operator in the  $\Delta$  as :

$$\langle P^+, \frac{\vec{q}_\perp}{2}, \lambda' | J^+(0) | P^+, -\frac{\vec{q}_\perp}{2}, \lambda \rangle = (2P^+) e^{i(\lambda - \lambda')\phi_q} A_{\lambda' \lambda}(Q^2), \quad (24)$$

where  $\lambda, \lambda'$  denotes the  $\Delta$  light-front helicities, and where  $\vec{q}_\perp = Q(\cos \phi_q \hat{e}_x + \sin \phi_q \hat{e}_y)$ . The helicity form factors  $A_{\lambda' \lambda}$  depend on  $Q^2$  only and can equivalently be expressed in terms of  $F_{1,2,3,4}^*$  as :

$$\begin{aligned} A_{\frac{3}{2}\frac{3}{2}} &= A_{-\frac{3}{2}-\frac{3}{2}} = F_1^* - \frac{\tau}{2} F_3^*, \\ A_{\frac{3}{2}\frac{1}{2}} &= -A_{-\frac{3}{2}-\frac{1}{2}} = A_{-\frac{1}{2}-\frac{3}{2}} = -A_{\frac{1}{2}\frac{3}{2}} = \frac{\tau^{1/2}}{\sqrt{3}} \left[ 2F_1^* - F_2^* - \tau \left( F_3^* - \frac{1}{2} F_4^* \right) \right], \\ A_{\frac{3}{2}-\frac{1}{2}} &= A_{-\frac{3}{2}\frac{1}{2}} = A_{-\frac{1}{2}\frac{3}{2}} = A_{\frac{1}{2}-\frac{3}{2}} = \frac{\tau}{\sqrt{3}} \left[ -2F_2^* + \frac{1}{2} F_3^* + \tau F_4^* \right], \\ A_{\frac{3}{2}-\frac{3}{2}} &= -A_{-\frac{3}{2}\frac{3}{2}} = -\frac{1}{2} \tau^{3/2} F_4^*, \\ A_{\frac{1}{2}\frac{1}{2}} &= A_{-\frac{1}{2}-\frac{1}{2}} = \left( 1 - \frac{4}{3} \tau \right) F_1^* + \frac{\tau}{3} \left[ 4F_2^* - \left( \frac{1}{2} - 2\tau \right) F_3^* - 2\tau F_4^* \right], \\ A_{\frac{1}{2}-\frac{1}{2}} &= -A_{-\frac{1}{2}\frac{1}{2}} = \frac{\tau^{1/2}}{3} \left[ 4F_1^* - 2(1 - 2\tau) F_2^* - 2\tau F_3^* + \tau \left( \frac{1}{2} - 2\tau \right) F_4^* \right]. \end{aligned} \quad (25)$$

Since the  $\Delta \rightarrow \Delta$  electromagnetic transition is described by four independent form factors, one finds two angular conditions among the helicity form factors of Eq. (25) :

$$\begin{aligned} 0 &= (1 + 4\tau) \sqrt{3} A_{\frac{3}{2}\frac{3}{2}} - 8\tau^{1/2} A_{\frac{3}{2}\frac{1}{2}} + 2A_{\frac{3}{2}-\frac{1}{2}} - \sqrt{3} A_{\frac{1}{2}\frac{1}{2}}, \\ 0 &= 4\tau^{3/2} A_{\frac{3}{2}\frac{3}{2}} + \sqrt{3}(1 - 2\tau) A_{\frac{3}{2}\frac{1}{2}} + \frac{1}{2} A_{\frac{3}{2}-\frac{3}{2}} - \frac{3}{2} A_{\frac{1}{2}-\frac{1}{2}}. \end{aligned} \quad (26)$$



## 5. The transverse charge densities for a spin-3/2 particle

We define a quark charge density for a spin-3/2 particle, such as the  $\Delta(1232)$ , in a state of definite light-cone helicity  $\lambda$ , by the Fourier transform :

$$\begin{aligned}\rho_\lambda^\Delta(b) &\equiv \int \frac{d^2\vec{q}_\perp}{(2\pi)^2} e^{-i\vec{q}_\perp \cdot \vec{b}} \frac{1}{2P^+} \langle P^+, \frac{\vec{q}_\perp}{2}, \lambda | J^+ | P^+, \frac{-\vec{q}_\perp}{2}, \lambda \rangle \\ &= \int_0^\infty \frac{dQ}{2\pi} Q J_0(Qb) A_{\lambda\lambda}(Q^2).\end{aligned}\quad (27)$$

The two independent quark charge densities for a spin-3/2 state of definite helicity are given by  $\rho_{\frac{3}{2}}^\Delta(b)$  and  $\rho_{\frac{1}{2}}^\Delta(b)$ . Note that for a pointlike particle, the ‘natural’ values of Eq. (22) lead to  $A_{\frac{3}{2}\frac{3}{2}}(Q^2) = 1$ , implying

$$\rho_{\frac{3}{2}}^\Delta(\vec{b}) = \delta^2(\vec{b}).\quad (28)$$

The above charge densities provide us with two combinations of the four independent  $\Delta$  FFs. To get information from the other FFs, we consider the charge densities in a spin-3/2 state with transverse spin. We denote this transverse polarization direction by  $\vec{S}_\perp = \cos\phi_S \hat{e}_x + \sin\phi_S \hat{e}_y$ , and the  $\Delta$  spin projection along the direction of  $\vec{S}_\perp$  by  $s_\perp$ . We first express the transverse spin basis in terms of the helicity basis for spin-3/2. For the states of transverse spin  $s_\perp = \frac{3}{2}$  and  $s_\perp = \frac{1}{2}$  this yields :

$$\begin{aligned}|s_\perp = +\frac{3}{2}\rangle &= \frac{1}{\sqrt{8}} \left\{ e^{-i\phi_S} |\lambda = +\frac{3}{2}\rangle + \sqrt{3} |\lambda = +\frac{1}{2}\rangle \right. \\ &\quad \left. + \sqrt{3} e^{i\phi_S} |\lambda = -\frac{1}{2}\rangle + e^{2i\phi_S} |\lambda = -\frac{3}{2}\rangle \right\}, \\ |s_\perp = +\frac{1}{2}\rangle &= \frac{1}{\sqrt{8}} \left\{ \sqrt{3} e^{-i\phi_S} |\lambda = +\frac{3}{2}\rangle + |\lambda = +\frac{1}{2}\rangle \right. \\ &\quad \left. - e^{i\phi_S} |\lambda = -\frac{1}{2}\rangle - \sqrt{3} e^{2i\phi_S} |\lambda = -\frac{3}{2}\rangle \right\},\end{aligned}\quad (29)$$

where the states on the *rhs* are the spin-3/2 helicity eigenstates.

We can then define the charge densities in a spin-3/2 state with transverse spin  $s_\perp$  as :

$$\rho_{T s_\perp}^\Delta(\vec{b}) \equiv \int \frac{d^2\vec{q}_\perp}{(2\pi)^2} e^{-i\vec{q}_\perp \cdot \vec{b}} \frac{1}{2P^+} \langle P^+, \frac{\vec{q}_\perp}{2}, s_\perp | J^+(0) | P^+, -\frac{\vec{q}_\perp}{2}, s_\perp \rangle. \quad (30)$$

By working out the Fourier transform in Eq. (30) for the two cases where  $s_\perp = \frac{3}{2}$

and  $s_{\perp} = \frac{1}{2}$ , using the  $\Delta$  helicity form factors of Eq. (25), one obtains :

$$\begin{aligned} \rho_T^{\Delta \frac{3}{2}}(\vec{b}) = \int_0^{+\infty} \frac{dQ}{2\pi} Q \quad & \left[ \begin{aligned} & J_0(Qb) \frac{1}{4} \left( A_{\frac{3}{2}\frac{3}{2}} + 3A_{\frac{1}{2}\frac{1}{2}} \right) \\ & - \sin(\phi_b - \phi_S) J_1(Qb) \frac{1}{4} \left( 2\sqrt{3}A_{\frac{3}{2}\frac{1}{2}} + 3A_{\frac{1}{2}-\frac{1}{2}} \right) \\ & - \cos[2(\phi_b - \phi_S)] J_2(Qb) \frac{\sqrt{3}}{2} A_{\frac{3}{2}-\frac{1}{2}} \\ & + \sin[3(\phi_b - \phi_S)] J_3(Qb) \frac{1}{4} A_{\frac{3}{2}-\frac{3}{2}} \end{aligned} \right], \end{aligned} \quad (31)$$

and

$$\begin{aligned} \rho_T^{\Delta \frac{1}{2}}(\vec{b}) = \int_0^{+\infty} \frac{dQ}{2\pi} Q \quad & \left[ \begin{aligned} & J_0(Qb) \frac{1}{4} \left( 3A_{\frac{3}{2}\frac{3}{2}} + A_{\frac{1}{2}\frac{1}{2}} \right) \\ & - \sin(\phi_b - \phi_S) J_1(Qb) \frac{1}{4} \left( 2\sqrt{3}A_{\frac{3}{2}\frac{1}{2}} - A_{\frac{1}{2}-\frac{1}{2}} \right) \\ & + \cos[2(\phi_b - \phi_S)] J_2(Qb) \frac{\sqrt{3}}{2} A_{\frac{3}{2}-\frac{1}{2}} \\ & - \sin[3(\phi_b - \phi_S)] J_3(Qb) \frac{3}{4} A_{\frac{3}{2}-\frac{3}{2}} \end{aligned} \right], \end{aligned} \quad (32)$$

where we defined the angle  $\phi_b$  in the transverse plane as,  $\vec{b} = b(\cos \phi_b \hat{e}_x + \sin \phi_b \hat{e}_y)$ . One notices from Eqs. (31,32) that the transverse charge densities display monopole, dipole, quadrupole, and octupole field patterns, which are determined by the helicity form factors with zero, one, two, or three units of helicity flip respectively between the initial and final  $\Delta$  states.

It is instructive to evaluate the electric dipole moment (EDM) corresponding to the transverse charge densities  $\rho_T^{\Delta s_{\perp}}$ , which is defined as :

$$\vec{d}_{s_{\perp}}^{\Delta} \equiv e \int d^2\vec{b} \vec{b} \rho_T^{\Delta s_{\perp}}(\vec{b}). \quad (33)$$

Eqs. (31,32) yield :

$$\vec{d}_{\frac{3}{2}}^{\Delta} = 3 \vec{d}_{\frac{1}{2}}^{\Delta} = - \left( \vec{S}_{\perp} \times \hat{e}_z \right) \{ G_{M1}(0) - 3e_{\Delta} \} \left( \frac{e}{2M_{\Delta}} \right). \quad (34)$$

Expressing the spin-3/2 magnetic moment in terms of the  $g$ -factor gives  $G_{M1}(0) = g \frac{3}{2} e_{\Delta}$ , so that the induced EDM  $\vec{d}_{s_{\perp}}^{\Delta}$  is proportional to  $g - 2$ . The same result was found before for the case of spin-1/2 particles in [6] and spin-1 particles in Ref. [7]. One thus observes as a universal feature that for a particle without internal structure (corresponding with  $g = 2$  [22, 23]), there is no induced EDM.

We next evaluate the electric quadrupole moment corresponding to the transverse charge densities  $\rho_T^{\Delta s_{\perp}}$ . Choosing  $\vec{S}_{\perp} = \hat{e}_x$ , the electric quadrupole moment can be defined as :

$$Q_{s_{\perp}}^{\Delta} \equiv e \int d^2\vec{b} (b_x^2 - b_y^2) \rho_T^{\Delta s_{\perp}}(\vec{b}). \quad (35)$$

From Eqs. (31,32) one obtains :

$$Q_{\frac{3}{2}}^{\Delta} = -Q_{\frac{1}{2}}^{\Delta} = \frac{1}{2} \{2 [G_{M1}(0) - 3e_{\Delta}] + [G_{E2}(0) + 3e_{\Delta}]\} \left( \frac{e}{M_{\Delta}^2} \right). \quad (36)$$

We note that for a spin-3/2 particle without internal structure, for which  $G_{M1}(0) = 3e_{\Delta}$  and  $G_{E2}(0) = -3e_{\Delta}$  according to Eq. (23), the quadrupole moment of the transverse charge densities vanishes. It is thus interesting to observe from Eq. (36) that  $Q_{s_{\perp}}^{\Delta}$  is only sensitive to the anomalous parts of the spin-3/2 magnetic dipole and electric quadrupole moments, and vanishes for a particle without internal structure. The same observation was made for the case of a spin-1 particle in Ref. [7].

At this point, it is important to emphasize the difference between densities and quadrupole moments defined in the lab and infinite momentum frames, and to discuss qualitatively the difference between Eq. (8c) and Eq. (36). For QCD in the lab frame, vacuum quark and gluon condensates as well as backward quark propagators play important roles in hadron structure. In contrast, the infinite momentum frame has neither condensates nor backward going propagators Feynman diagrams. To boost a state from the lab to the infinite momentum frame is as complicated as solving for the state in either frame, so at best, the effect of boosts can only be described in models. Because deep inelastic scattering naturally specifies quark distributions and transverse densities in the infinite momentum frame, and because of the wealth of experimental information about parton distributions and generalized parton distributions, it is clearly valuable to develop a physical understanding of and intuition for distributions and densities in this frame, and the extraction of transverse densities from form factors can contribute substantially to this understanding and intuition. However, at the same time, it is essential to treat densities in this frame as physically distinct from those in the lab.

In this context, it is useful to discuss three differences between the conventional quadrupole moment  $Q_{\Delta}$  of the three-dimensional density in the lab frame, Eq. (8c), and the quadrupole moment  $Q_{s_{\perp}}^{\Delta}$  in the infinite momentum frame, Eq. (36). The factor  $[G_{M1}(0) - 3e_{\Delta}]$  is an electric quadrupole moment induced in the moving frame due to the magnetic dipole moment, which is obviously absent in the lab. As discussed previously, the combination  $[G_{E2}(0) + 3e_{\Delta}]$  in Eq. (36) arises in the infinite momentum frame to describe non-point-like structure because the value for a point particle is  $-3e_{\Delta}$ , whereas no such term is pertinent in the lab.

Finally, the overall factor 1/2 in Eq. (36) can be understood qualitatively by ignoring the distinction between the densities in the lab and infinite momentum frame, and considering a hypothetical limit in which one has a 3-dimensional density that is axially symmetric around the  $x$  axis and the transverse two-dimensional density is just the 2-dimensional projection of this density, without any change of physics between the lab and infinite momentum frames. Taking the spin axis along the  $x$  axis, the quadrupole moment  $Q_{3d}$  of the 3-dimensional

distribution is defined as :

$$\begin{aligned} Q_{3d} &\equiv \int dx dy dz (3x^2 - r^2) \rho_{3d}(x, y, z), \\ &= \int dx dy dz [(x^2 - y^2) + (x^2 - z^2)] \rho_{3d}(x, y, z). \end{aligned} \quad (37)$$

For a 3-dimensional charge distribution that is invariant under rotations around the axis of the spin, the two terms proportional to  $(x^2 - y^2)$  and  $(x^2 - z^2)$  in Eq. (37) give equal contributions yielding :

$$Q_{3d} = 2 \int dx dy dz (x^2 - y^2) \rho_{3d}(x, y, z). \quad (38)$$

Introducing the 2-dimensional charge density in the  $xy$ -plane as :

$$\rho_{2d}(x, y) = \int dz \rho_{3d}(x, y, z), \quad (39)$$

one immediately obtains the relation

$$Q_{3d} = 2 Q_{2d}, \quad (40)$$

with the quadrupole moment of the 2-dimensional charge density defined as :

$$Q_{2d} \equiv \int dx dy (x^2 - y^2) \rho_{2d}(x, y). \quad (41)$$

Because  $Q_{3d}$  is proportional to  $G_{E2}(0)$  in our hypothetical case, we see that Eq. (40) yields a  $Q_{2d}$  that is half the value of  $G_{E2}(0)$ , consistent with Eq. (36). We will return to the differences between physics in the lab and infinite momentum frames and between Eq. (8c) and Eq. (36) in the discussion of models in the final section.

In the same way as for the quadrupole moment, we can also evaluate the electric octupole moment corresponding with the transverse charge densities  $\rho_{T s_\perp}^\Delta$ . Choosing  $\vec{S}_\perp = \hat{e}_x$ , the electric octupole moment can be defined as :

$$\begin{aligned} O_{s_\perp}^\Delta &\equiv e \int d^2 \vec{b} b^3 \sin(3\phi_b) \rho_{T s_\perp}^\Delta(\vec{b}), \\ &= e \int d^2 \vec{b} b_y (3b_x^2 - b_y^2) \rho_{T s_\perp}^\Delta(\vec{b}). \end{aligned} \quad (42)$$

From Eqs. (31,32) one obtains :

$$O_{\frac{3}{2}}^\Delta = -\frac{1}{3} O_{\frac{1}{2}}^\Delta = \frac{3}{2} \left\{ -G_{M1}(0) - G_{E2}(0) + G_{M3}(0) + e_\Delta \right\} \left( \frac{e}{2M_\Delta^3} \right) \quad (43)$$

We note that for a spin-3/2 particle without internal structure, for which  $G_{M1}(0) = 3e_\Delta$ ,  $G_{E2}(0) = -3e_\Delta$ , and  $G_{M3}(0) = -e_\Delta$  according to Eq. (23), the electric octupole moment of the transverse charge densities vanishes.

## 6. Lattice calculation for the $\Delta(1232)$ e.m. form factors

Since the  $\Delta(1232)$  e.m. FFs are not known experimentally, apart from the scarce phenomenological information described in Section 2, we will rely on recent lattice QCD calculations [29] for these FFs. For the  $\Delta$  magnetic dipole moment, first dynamical results, using a background field method, with  $N_F = 2+1$  quark flavors were presented in Ref. [30]. For the  $\Delta$  e.m. FFs, first dynamical results were presented in Ref. [11]. We will discuss the latter calculations in more detail in the present section.

We use three types of simulations that we refer to as SIM-I, SIM-II and SIM-III. In the SIM-I simulations, we use Wilson fermions and the standard Wilson plaquette gauge-action in the quenched approximation. In the SIM-II simulations, we use two dynamical degenerate flavors of Wilson fermions and the standard Wilson plaquette gauge-action. Finally, in the SIM-III simulations, we use the following mixed action scheme. For the dynamical sea quarks, we use the staggered Asqtad action by the MILC collaboration [31] and include two degenerate flavors of light quarks plus strange quarks. The strange quark mass is fixed to the physical strange quark mass. For the valence quarks we use domain wall fermions (DWF) that preserve a form of chiral symmetry on the lattice. The domain wall quark mass takes the values given in Tables 1 and has been tuned by adjusting the lightest pseudoscalar meson in the Asqtad calculation [31] to have the same mass as the pseudoscalar meson using domain-wall fermions. Technical details of this tuning procedure are given in Refs. [32, 33]. Using this mixed action, a number of interesting observables were recently evaluated, including the nucleon axial charge, where hybrid action chiral extrapolation to the physical point has been carried out [34] and moments of generalized form factors, which are also chirally extrapolated[33].

In this work we present a comparison between results with dynamical fermions obtained using the Wilson and the domain wall fermion discretization schemes. For finite lattice spacings these are different actions and agreement between them provides a non-trivial check of lattice cutoff effects. Results in the quenched approximation have the advantage that they are easily produced and have smaller statistical errors. Therefore they can be used to optimize the construction of the three point functions. In addition, comparison with the unquenched data at a similar pion mass provides a measure of unquenching effects. For all simulations considered in this work the  $\Delta$  is a stable particle. On the lattice we calculate the form factors  $G_{E0}$ ,  $G_{E2}$ ,  $G_{M1}$  and  $G_{M3}$  of which the electric charge,  $G_{E0}$ , and the magnetic dipole,  $G_{M1}$ , form factors are dominant.

### 6.1. Ground state dominance

We use an interpolating field with the quantum numbers of the  $\Delta^+$  baryon to create an initial state from the vacuum with non-zero overlap with the  $\Delta^+$ -state. The standard interpolating field that reduces to the quark-model wave

function in the non-relativistic limit is given by

$$\chi_{\sigma\alpha}^{\Delta^+}(x) = \frac{1}{\sqrt{3}}\epsilon^{abc} \left[ 2 (\mathbf{u}^{a\top}(x) C \gamma_\sigma \mathbf{d}^b(x)) \mathbf{u}_\alpha^c(x) + (\mathbf{u}^{a\top}(x) C \gamma_\sigma \mathbf{u}^b(x)) \mathbf{d}_\alpha^c(x) \right], \quad (44)$$

where  $C$  is the charge conjugation matrix. We note that this interpolating field creates both a spin-3/2 and a spin-1/2 state. However the overlap of this interpolating field with the spin-1/2  $\Delta^+$  that is higher in energy is very much suppressed and has negligible contribution to the correlator functions [35]. The overlap of the interpolating field with the spin-3/2  $\Delta^+$  is

$$\langle \Omega | \chi_{\sigma\alpha}(0) | \Delta(p, s) \rangle = Z u_{\sigma\alpha}(p, s), \quad \langle \Delta(p, s) | \bar{\chi}_{\sigma\alpha}(0) | \Omega \rangle = Z^* \bar{u}_{\sigma\alpha}(p, s), \quad (45)$$

and as in Eq. (1)  $u_\sigma$  denotes a Rarita-Schwinger spinor. Every vector component of this vector-spinor solves the free Dirac equation

$$[\not{p} - M_\Delta] u_\sigma(p, s) = 0, \quad (46)$$

and in addition the two auxiliary conditions

$$p_\sigma u^\sigma(p, s) = 0 \quad \text{and} \quad \gamma_\sigma u^\sigma(p, s) = 0 \quad (47)$$

are satisfied. The well known expression for the spin-sum is given by

$$\begin{aligned} \Lambda_{\sigma\tau} &\equiv \sum_{s=-3/2}^{3/2} u_\sigma(p, s) \bar{u}_\tau(p, s) \\ &= -\frac{\not{p} + M_\Delta}{2M_\Delta} \left( g_{\sigma\tau} - \frac{\gamma_\sigma \gamma_\tau}{3} - \frac{2p_\sigma p_\tau}{3M_\Delta^2} + \frac{p_\sigma \gamma_\tau - p_\tau \gamma_\sigma}{3M_\Delta} \right), \end{aligned} \quad (48)$$

using the normalization  $\bar{u}^\alpha u_\alpha = -1$ .

To facilitate ground-state dominance, we employ a covariant Gaussian smearing [36] on the quark-fields entering Eq. (44)

$$\mathbf{q}_\beta(t, \vec{x}) = \sum_{\vec{y}} [\mathbf{1} + \alpha H(\vec{x}, \vec{y}; U)]^n q_\beta(t, \vec{y}) \quad (49)$$

$$H(\vec{x}, \vec{y}; U) = \sum_{\mu=1}^3 (U_\mu(\vec{x}, t) \delta_{\vec{x}, \vec{y}-\hat{\mu}} + U_\mu^\dagger(\vec{x} - \hat{\mu}, t) \delta_{\vec{x}, \vec{y}+\hat{\mu}}) \quad (50)$$

Here  $q$  is the local  $u$  or  $d$  quark field,  $\mathbf{q}$  is the smeared quark field and  $U_\mu$  is the  $SU(3)$ -gauge field. For the lattice spacings and pion masses considered in this work, the values  $\alpha = 4.0$  and  $n = 50$  ensure ground state dominance with the shortest time evolution that could be achieved.

## 6.2. Correlation functions

While the Breit frame is suitable for the introduction of multipole form factors, and the infinite momentum frame allows for a clean definition of transverse charge densities, we find that the most convenient kinematical setup for

the lattice calculation is one where the final  $\Delta$ -state is at rest ( $\vec{p}_f = \vec{0}$ ). Furthermore, since lattice calculations are carried out in a Euclidean space-time, for the remainder of this chapter, all expressions are given with Euclidean conventions [37].

We consider two-point and three-point functions constructed from the interpolating fields defined in Eq. (44) ,

$$G_{\sigma\tau}(\Gamma^\nu, \vec{p}, t) = \sum_{\vec{x}_f} e^{-i\vec{x}_f \cdot \vec{p}} \Gamma_{\alpha'\alpha}^\nu \left\langle \chi_{\sigma\alpha}(t, \vec{x}_f) \bar{\chi}_{\tau\alpha'}(0, \vec{0}) \right\rangle, \quad (51)$$

$$G_{\sigma\mu\tau}(\Gamma^\nu, \vec{q}, t) = \sum_{\vec{x}, \vec{x}_f} e^{i\vec{x} \cdot \vec{q}} \Gamma_{\alpha'\alpha}^\nu \left\langle \chi_{\sigma\alpha}(t_f, \vec{x}_f) V_\mu(t, \vec{x}) \bar{\chi}_{\tau\alpha'}(0, \vec{0}) \right\rangle. \quad (52)$$

With lattice Wilson fermions,  $V_\mu$  is the symmetrized, conserved electromagnetic current given by

$$V_\mu(x) = \frac{2}{6} (j_\mu^u(x) + j_\mu^u(x - \hat{\mu})) - \frac{1}{6} (j_\mu^d(x) + j_\mu^d(x - \hat{\mu})) \quad \text{where} \quad (53)$$

$$j_\mu^q(x) = \bar{q}(x + \hat{\mu}) \frac{1}{2} [\gamma_\mu + \mathbb{1}] U_\mu^{-1}(x) q(x) + \bar{q}(x) \frac{1}{2} [\gamma_\mu - \mathbb{1}] U_\mu(x) q(x + \hat{\mu}). \quad (54)$$

In the hybrid calculation we use the local vector current and determine the renormalization constant  $Z_V$  by the condition  $G_E(0) = 1$  (in units of the electric charge) for the  $\Delta^+$ . The  $\Gamma$  matrices are given by

$$\Gamma^4 = \frac{1}{4} (\mathbb{1} + \gamma^4), \quad \Gamma^k = \frac{i}{4} (\mathbb{1} + \gamma^4) \gamma_5 \gamma_k, \quad k = 1, 2, 3. \quad (55)$$

By inserting into the correlation functions complete sets of energy momentum eigenstates

$$\sum_{n,p,\xi} \frac{M_n}{V E_{n(p)}} |n(p, \xi)\rangle \langle n(p, \xi)| = \mathbb{1} \quad , \quad (56)$$

with  $\xi$  denoting all other quantum numbers like spin and its projection on some axis, one finds that the leading contributions for large Euclidean times  $t$  and  $t_f - t$  are

$$\begin{aligned} G_{\sigma\tau}(\Gamma^\nu, \vec{p}, t) &= \frac{M_\Delta}{E_{\Delta(p)}} |Z|^2 e^{-E_{\Delta(p)} t} \text{tr} [\Gamma^\nu \Lambda_{\sigma\tau}^E(p)] + \text{excited states}, \quad (57) \\ G_{\sigma\mu\tau}(\Gamma^\nu, \vec{q}, t) &= \frac{M_\Delta}{E_{\Delta(p_i)}} |Z|^2 e^{-M_\Delta (t_f - t)} e^{-E_{\Delta(p_i)} t} \text{tr} [\Gamma^\nu \Lambda_{\sigma\sigma'}^E(p_f) \mathcal{O}_{\sigma'\mu\tau'}^E \Lambda_{\tau'\tau}^E(p_i)] \\ &+ \text{excited states}. \quad (58) \end{aligned}$$

To calculate the spin traces, the Euclidean versions of Eq. (1) and Eq. (48) are employed. The unknown overlap  $Z$ -factors and the leading time dependence cancel in certain ratios of three- and two- point functions. Our preferred choice is the ratio

$$R_{\sigma\mu\tau}(\Gamma, \vec{q}, t) = \frac{G_{\sigma\mu\tau}(\Gamma, \vec{q}, t)}{G_{kk}(\Gamma^4, \vec{0}, t_f)} \sqrt{\frac{G_{kk}(\Gamma^4, \vec{p}_i, t_f - t) G_{kk}(\Gamma^4, \vec{0}, t) G_{kk}(\Gamma^4, \vec{0}, t_f)}{G_{kk}(\Gamma^4, \vec{0}, t_f - t) G_{kk}(\Gamma^4, \vec{p}_i, t) G_{kk}(\Gamma^4, \vec{p}_i, t_f)}}, \quad (59)$$

with implicit summations over the indices  $k$  with  $k = 1, 2, 3$ . It becomes time independent for large Euclidean time separations  $t_f - t$  and  $t$ :

$$R_{\sigma\mu\tau}(\Gamma, \vec{q}, t) \rightarrow \Pi_{\sigma\mu\tau}(\Gamma, \vec{q}) = C \operatorname{tr} [\Gamma \Lambda_{\sigma\sigma'}(p_f) \mathcal{O}_{\sigma'\mu\tau'} \Lambda_{\tau'\tau}(p_i)] , \quad (60)$$

with

$$C \equiv \sqrt{\frac{3}{2}} \left[ \frac{2E_{\Delta}(p_i)}{M_{\Delta}} + \frac{2E_{\Delta}^2(p_i)}{M_{\Delta}^2} + \frac{E_{\Delta}^3(p_i)}{M_{\Delta}^3} + \frac{E_{\Delta}^4(p_i)}{M_{\Delta}^4} \right]^{-\frac{1}{2}} , \quad (61)$$

stemming from the state normalization and the 2-point function traces.

Since we are evaluating the correlator of Eq. (52) using sequential inversions through the sink [38], a separate set of inversions is necessary for every choice of vector and Dirac-indices. The total of 256 combinations is beyond our computational resources, and hence we concentrate on a few carefully chosen combinations given below:

$$\begin{aligned} \Pi_{\mu}^{(1)}(\vec{q}) &= \sum_{j,k,l=1}^3 \epsilon_{jkl} \Pi_{j\mu k}(\Gamma^4, \vec{q}) \\ &= G_{M1} \frac{5i(E_{\Delta} + M_{\Delta})C}{18M_{\Delta}^2} [\delta_{1,\mu}(q_3 - q_2) + \delta_{2,\mu}(q_1 - q_3) + \delta_{3,\mu}(q_2 - q_1)] , \end{aligned} \quad (62)$$

$$\begin{aligned} \Pi_{\mu}^{(2)}(\vec{q}) &= \sum_{k=1}^3 \Pi_{k\mu k}(\Gamma^4, \vec{q}) \\ &= -G_{E0} \frac{(E_{\Delta} + 2M_{\Delta})C}{3M_{\Delta}^2} [(M_{\Delta} + E_{\Delta})\delta_{4,\mu} + iq_{\mu}(1 - \delta_{4,\mu})] \\ &\quad - G_{E2} \frac{(E_{\Delta} - M_{\Delta})^2 C}{9M_{\Delta}^3} [(M_{\Delta} + E_{\Delta})\delta_{4,\mu} + iq_{\mu}(1 - \delta_{4,\mu})] , \end{aligned} \quad (63)$$

$$\begin{aligned} \Pi_{\mu}^{(3)}(\vec{q}) &= \sum_{j,k,l=1}^3 \epsilon_{jkl} \Pi_{j\mu k}(\Gamma^j, \vec{q}) \\ &= G_{E2} \frac{-iC}{3M_{\Delta}^2(E_{\Delta} + M_{\Delta})} (q_1 q_2 + q_2 q_3 + q_3 q_1) \\ &\quad \times [(M_{\Delta} + E_{\Delta})\delta_{4,\mu} + iq_{\mu}(1 - \delta_{4,\mu})] \\ &\quad + G_{M1} \frac{C}{6M_{\Delta}^2(E_{\Delta} + M_{\Delta})} \sum_{k=1}^3 \delta_{k,\mu} q_1 q_2 q_3 \left( 2 - \frac{q_1 + q_2 + q_3 - q_k}{q_k} \right) \\ &\quad + G_{M3} \frac{C}{30M_{\Delta}^3(E_{\Delta} + M_{\Delta})} \sum_{k=1}^3 \delta_{k,\mu} \left[ (16E_{\Delta} + 14M_{\Delta})q_1 q_2 q_3 \right. \\ &\quad \quad - 10M_{\Delta}(q_1 q_2 + q_2 q_3 + q_3 q_1)q_k \\ &\quad \quad \left. - (8E_{\Delta} + 7M_{\Delta}) \frac{q_1 q_2 q_3}{q_k} (q_1 + q_2 + q_3 - q_k) \right] . \end{aligned} \quad (64)$$



As expected, current conservation  $q_\mu \Pi_\mu = 0$  is manifest in the right hand side of the equations. From these expressions, all the multipole form factors can be extracted. For instance, Eq. (62) is proportional to  $G_{M1}$ , while Eq. (64) isolates  $G_{E2}$  for  $\mu = 4$ . Furthermore, these combinations are optimal in the sense that all momentum directions, each of which is statistically different, contribute to a given  $Q^2$ -value. This symmetric construction yields a better estimator for the  $\Delta$ -matrix elements than methods where only one momentum-vector is accessible.

Wilson fermions						
V	# confs	$\kappa$	$m_\pi$ (GeV)	$m_\pi/m_\rho$	$m_N$ (GeV)	$m_\Delta$ (GeV)
SIM-I : Quenched, $\beta = 6.0$ , $a^{-1} = 2.14(6)$ GeV						
$32^3 \times 64$	200	0.1554	0.563(4)	0.645(9)	1.267(11)	1.470(15)
$32^3 \times 64$	200	0.1558	0.490(4)	0.587(12)	1.190(13)	1.425(16)
$32^3 \times 64$	200	0.1562	0.411(4)	0.503(23)	1.109(13)	1.382(19)
SIM-II: Unquenched, $\beta = 5.6$ , $a^{-1} = 2.56(10)$ GeV						
$24^3 \times 40$	185 [39]	0.1575	0.691(8)	0.701(9)	1.485(18)	1.687(15)
$24^3 \times 40$	157 [39]	0.1580	0.509(8)	0.566(12)	1.280(26)	1.559(19)
$24^3 \times 32$	200 [40]	0.15825	0.384(8)	0.453(27)	1.083(18)	1.395(18)
SIM-III: Mixed action						
Asqtad ( $am_{u,d/s} = 0.01/0.05$ ), DWF ( $am_{u,d} = 0.0138$ ), $a^{-1} = 1.58(3)$ GeV						
V	# confs		$m_\pi$ (GeV)	$m_\pi/m_\rho$	$m_N$ (GeV)	$m_\Delta$ (GeV)
$28^3 \times 64$	300		0.353(2)	0.368(8)	1.191(19)	1.533(27)

Table 1: Parameters used in the calculation of the form factors.

### 6.3. Sink-source separation

Apart from the simulations themselves, sequential inversions are the most time consuming part of the calculation. They are done by constructing an appropriate sequential source, which requires that we fix the initial and final hadron states as well as the sink-source time separation,  $t_f$ . Changing  $t_f$  requires a new set of sequential inversions. Therefore we must first determine the optimal value of  $t_f$ . The criterion is to choose  $t_f$  as small as possible so that statistical errors due to the exponential decrease of the signal are minimized but large enough so that we ensure that excited states with  $\Delta$  quantum numbers are suppressed when the photon couples to a quark at time  $t$  from the source. Smearing techniques are essential for attaining early ground state dominance as discussed in the previous subsection. The optimal source-sink separation for a very similar calculation to ours was determined in Refs. [10, 29]. The authors find that a distance of about 1 fm is sufficient to suppress excited state contributions well below our targeted statistical errors. This translates into a separation of 12 time slices for SIM-I, 13 for SIM-II and 8 for SIM-III. That this

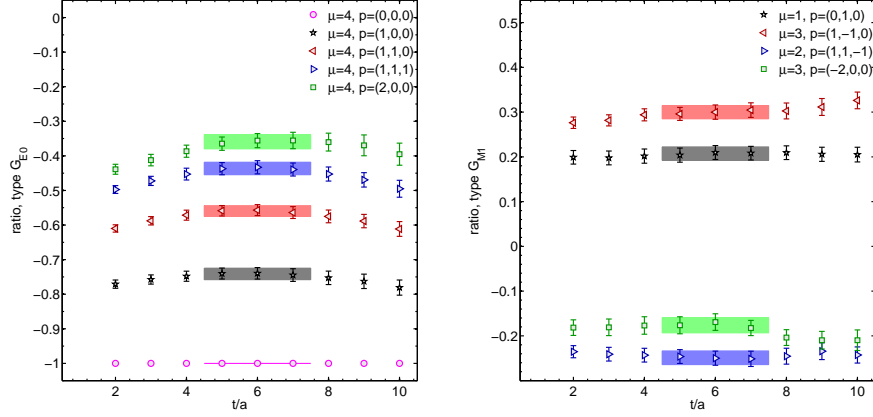


Figure 2: The ratio defined in Eq. (59) for a few of the lowest momenta. The left panel shows the combination from which  $G_{E0}$  is extracted, whereas the right shows the one that isolates  $G_{M1}$ . This is for the quenched case where due to the high statistical accuracy excited state contributions are most visible. For higher momenta, as well as for the suppressed form factors the ratio of systematic to statistical error is lower.

is indeed sufficient, is demonstrated in Fig. 2 and Fig. 3 where we show a few representative ratios with plateaus for SIM-I and SIM-III respectively.

#### 6.4. Volume dependence

Another potential source of systematic error is the spatial size of our lattices. Given that for the quenched case we use a lattice of spatial size about 3 fm, we expect finite volume effects to be negligible. Similarly, for the mixed action, the spatial lattice size is  $L_s = 3.5$  fm giving  $L_s m_\pi = 6.4$  ensuring small finite volume effects. In Ref. [10] it was in fact shown that for the N to  $\Delta$  matrix elements, finite volume effects are small for  $L_s m_\pi \gtrsim 4.5$ . Except for the lightest mass for dynamical Wilson fermions for which  $L_s m_\pi \sim 3.6$ , for all our quark masses we have  $L_s m_\pi > 4.6$ , and therefore we expect finite volume effects to be small.

#### 6.5. Data analysis

For a given value of  $Q^2$ , the combinations given in Eqs. (62) to (64) are evaluated for all different directions of  $\vec{q}$  resulting in this  $Q^2$ , as well as for all four directions  $\mu$  of the current. This leads to an over-constrained linear system of equations, which is then solved in the least-squares sense yielding estimates of  $G_{E0}$ ,  $G_{E2}$ ,  $G_{M1}$  and  $G_{M3}$ . This estimation is embedded into a jackknife binning procedure, thus providing statistical errors for the form factors that take all correlation and autocorrelation effects into account.

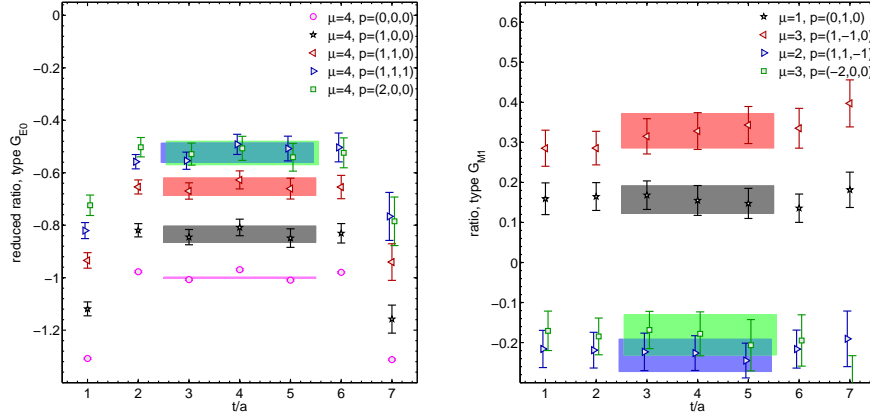


Figure 3: The same as in Fig. 2 but for the hybrid case.

### 6.6. Simulation parameters

The simulation parameters of our calculation are given in Table 1. In the case of Wilson fermions, the lattice spacing has been estimated using the nucleon mass in the chiral limit [41]. The value extracted using the nucleon mass is in agreement with the determination using the hadronic scale  $r_0$  defined via the force between static quarks at intermediate distance [42]. The lattice spacing in the case of staggered fermions has been determined from heavy-quark spectroscopy [43] as  $a = 0.1241$  fm with a statistical uncertainty of 2%. The calculation has been performed on relatively large lattices in the quenched approximation and in the case of the mixed action of spatial extent 2.9 fm and 3.4 fm respectively. On the other hand, in the case of dynamical Wilson fermions we use a finer lattice with a spatial size of only 1.9 fm.

Isospin symmetry relates results obtained for the  $\Delta^+$  to those for the  $\Delta^{++}$ ,  $\Delta^0$  and  $\Delta^-$  since they differ only by a charge-factor. The pion and  $\Delta$  masses corresponding to the three values of the hopping parameter,  $\kappa$ , considered in simulations SIM-I and SIM-II as well as the smallest available pion mass in the mixed action are summarized in Table 1. The results presented in the next subsection are obtained from the connected contributions to the full electromagnetic current. These yield the iso-vector form factors with the iso-vector current being given by  $V_\mu^I = \bar{u}\gamma_\mu u - \bar{d}\gamma_\mu d$ . In this case the disconnected diagrams cancel. The iso-scalar form factors have contributions from disconnected diagrams. At present, it is not yet computationally feasible to calculate the contributions arising from disconnected diagrams since they require the calculation of all-to-all propagators. An exact evaluation of all-to-all propagators requires spatial volume inversions for each time slice  $t$  that we are interested in. Such a computation is not feasible. Stochastic techniques have been developed to estimate all-to-all propagators [44]. Various improvements are being developed

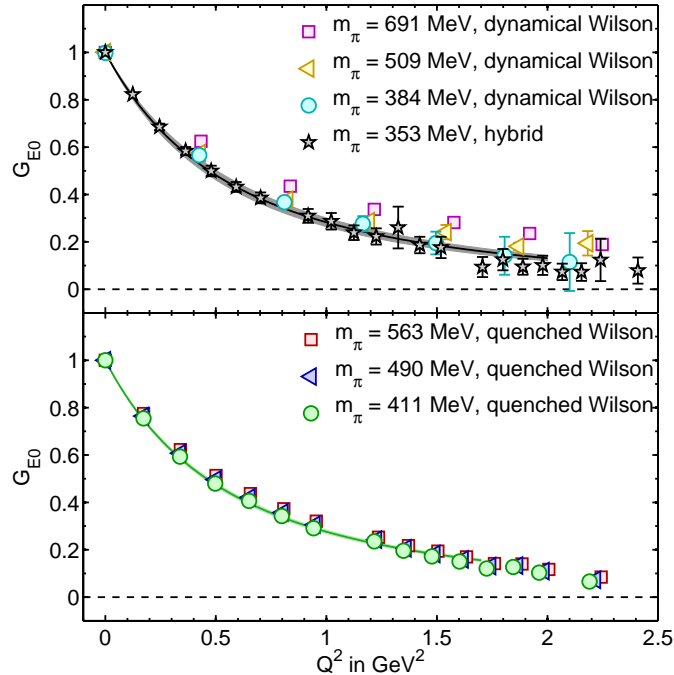


Figure 4: Comparison of three different QCD lattice calculations for the  $\Delta^+(1232)$  form factor  $G_{E0}$ . The upper curve is for SIM-II and SIM-III using dynamical quarks, whereas the lower curve is for SIM-I using the quenched approximation [29]. The lines show the fits to a dipole form of the lattice results at the smallest pion mass. For the case of dynamical quarks (upper graph) the fit is made to the results obtained using the mixed action. The error band is calculated using a jackknife analysis of the fit parameters.

in order to improve the measurements [45]. However, these disconnected contributions are particularly hard to calculate not just because they require the all-to-all propagators but also because they are noise-dominated [46]. A calculation of disconnected contributions in the case of the electromagnetic form factors have shown that these are consistent with zero within large statistical errors [47]. We expect that, like in the case of nucleon electromagnetic form factors, the disconnected contributions to the electromagnetic  $\Delta$  form factors are small. Therefore assuming that the disconnected diagrams are small then we obtain the electromagnetic form factors of  $\Delta$ .

### 6.7. Results

We show in Figs. 4 and 5 the two dominant Sachs form factors  $G_{E0}$  and  $G_{M1}$  as a function of the  $Q^2$  for all the light quark masses. In Fig. 6 we display

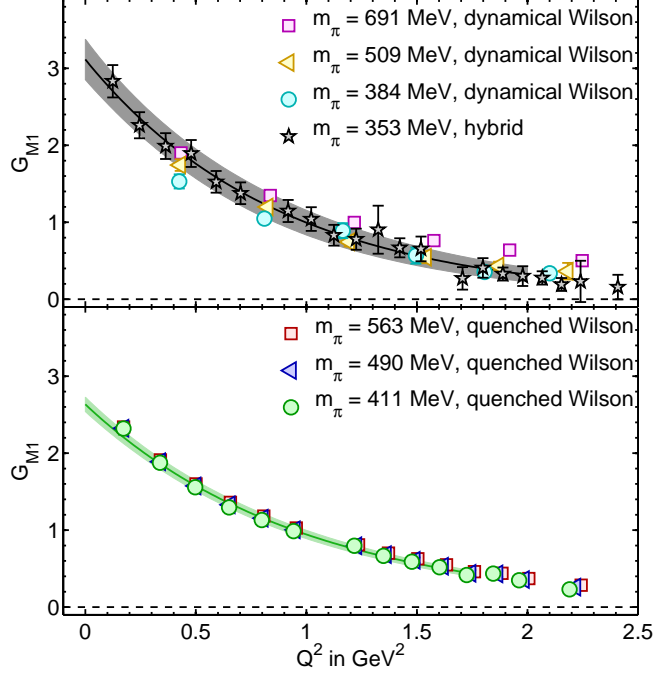


Figure 5: Comparison of three different QCD lattice calculations for the  $\Delta^+(1232)$  magnetic dipole form factors  $G_{M1}$ . The lines show the fits to an exponential form of the lattice results at the smallest pion mass. The rest of the notation is the same as that in Fig. 4.

the  $Q^2$ -dependence of the subdominant Sachs form factor  $G_{E2}$ . Their values are tabulated in Tables 3, 4 and 5 of the Appendix.

For  $G_{E0}$ , we consider a dipole parameterization of the lattice results :

$$G_{E0}(Q^2) = \frac{1}{(1 + Q^2/\Lambda_{E0}^2)^2}, \quad (65)$$

with  $\Lambda_{E0}^2$  treated as a free parameter. The choice of the parameterization for the  $\Delta$  multipole form factors given in Eq. (65) ensures that the helicity conserving form factors  $A_{\frac{3}{2}\frac{3}{2}}$  and  $A_{\frac{1}{2}\frac{1}{2}}$  behave as  $1/Q^4$  for large  $Q^2$ . For  $G_{M1}$  and  $G_{E2}$ , we instead consider exponential parameterizations with two free parameters for each since the expected large  $Q^2$ -dependence for these form factors is stronger than for a dipole :

$$\begin{aligned} G_{M1}(Q^2) &= G_{M1}(0) e^{-Q^2/\Lambda_{M1}^2}, \\ G_{E2}(Q^2) &= G_{E2}(0) e^{-Q^2/\Lambda_{E2}^2}. \end{aligned} \quad (66)$$

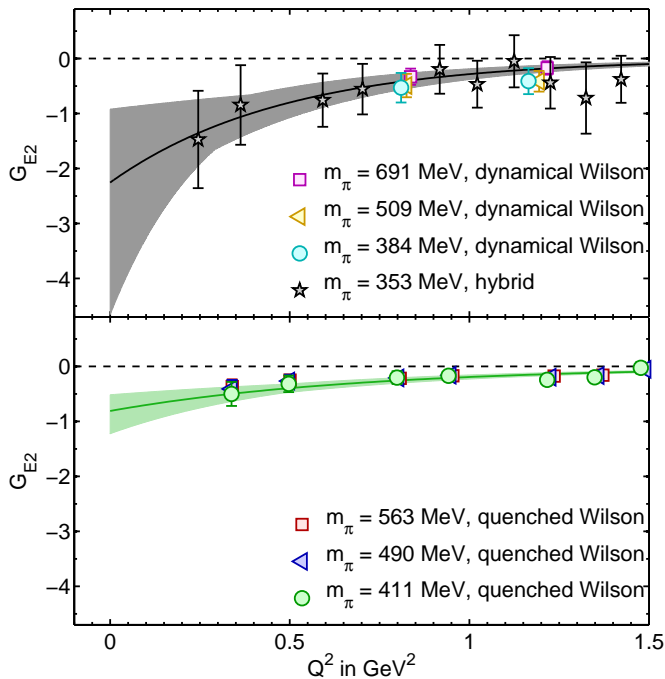


Figure 6: Comparison of three different QCD lattice calculations for the  $\Delta^+(1232)$  electric quadrupole form factors  $G_{E2}$ . The notation is the same as that in Fig. 5.

The magnetic octupole form factor  $G_{M3}$  evaluated in the quenched approximation [29] is found to have a small negative value albeit with large error. The results for  $G_{M3}$  using dynamical Wilson fermions obtained in this work are compatible with  $G_{M3}(Q^2) \simeq 0$  within the current statistical accuracy. We will therefore not discuss further lattice results for  $G_{M3}$ .

The values of the parameters entering the dipole fit of Eq. (65) for  $G_{E0}$ , and the exponential fits of Eq. (66) for  $G_{M1}$  and  $G_{E2}$ , fitted to the three different lattice calculations SIM-I, SIM-II and SIM-III are listed in Table 2.

In Figs. 4, 5 and 6 we show the fits to the lattice results for the form factors  $G_{E0}$ ,  $G_{M1}$  and  $G_{E2}$  for the smallest pion mass in each of the three type of simulations. One sees that for  $G_{E0}$  all three calculations give similar results. For  $G_{M1}$  and more so for  $G_{E2}$ , a larger spread in the resulting fits is observed. For  $G_{E2}(0)$  the hybrid lattice calculation yields a quadrupole moment consistent with the large- $N_c$  value, Eq. (16), whereas the quenched and dynamical  $N_f = 2$  Wilson calculations yield only about half this value. It should, however, be noted that the present dynamical calculations still have substantially larger error bars

	$m_\pi$ (GeV)	$\Lambda_{E0}^2$ (GeV <sup>2</sup> )	$G_{M1}(0)$	$\Lambda_{M1}^2$ (GeV <sup>2</sup> )	$G_{E2}(0)$	$\Lambda_{E2}^2$ (GeV <sup>2</sup> )
SIM-I	0.563(4)	1.243(27)	2.695(59)	1.015(32)	-0.46(20)	1.06(42)
	0.490(4)	1.173(28)	2.678(72)	0.994(36)	-0.52(26)	0.91(39)
	0.411(4)	1.109(29)	2.635(94)	0.975(23)	-0.81(29)	0.696(200)
SIM-II	0.691(8)	1.667(106)	2.589(78)	1.300(81)	-0.71(49)	1.00(64)
	0.509(8)	1.318(48)	2.68(13)	0.977(74)	-1.68(88)	0.76(30)
	0.384(8)	1.144(54)	2.35(16)	1.015(76)	-0.87(67)	1.75(1.39)
SIM-III	0.353(2)	1.160(78)	3.04(24)	0.935(122)	$-2.06^{+1.27}_{-2.35}$	$0.54^{+1.69}_{-0.25}$

Table 2: Parameters for the  $\Delta^+(1232)$  FFs for three different lattice QCD calculations : quenched Wilson (SIM-I), dynamical  $N_f = 2$  Wilson (SIM-II), and a hybrid calculation (SIM-III) described in the text. For  $G_{E0}$ , the dipole parameterization of Eq. (65) is used. For  $G_{M1}$  and  $G_{E2}$ , the exponential parameterization of Eq. (66) is used. The errors on the parameters are jackknife errors.

than the quenched calculations.

## 7. The $\Delta^+$ transverse densities

In this section, we will use the values of the parameters determined in the lattice fits to the  $\Delta$  e.m. FFs, discussed in Section 6, to evaluate the quark transverse densities in the  $\Delta^+(1232)$ .

In Fig. 7, we compare the  $\Delta^+$  transverse densities in helicity states of  $\lambda = 3/2$  and  $\lambda = 1/2$ , using Eq. (27), for the quenched lattice calculations. A comparison reveals that both are very similar, showing a positive core in the transverse charge density of about 0.7 fm. One notices that the quark transverse density in a  $\lambda = 1/2$  state is slightly more concentrated than its  $\lambda = 3/2$  counterpart.

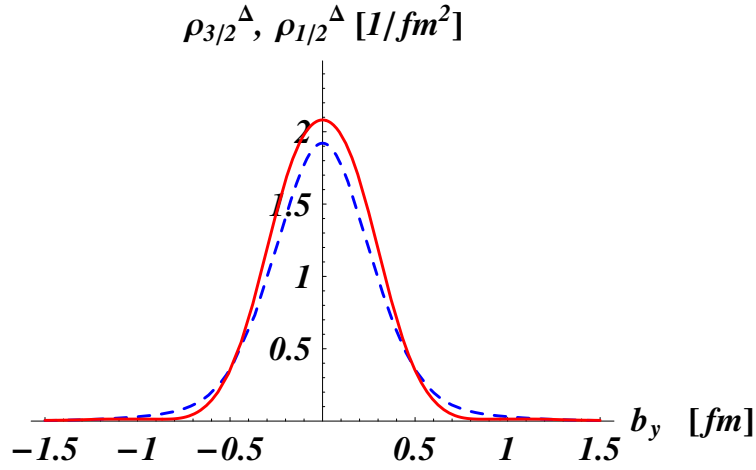
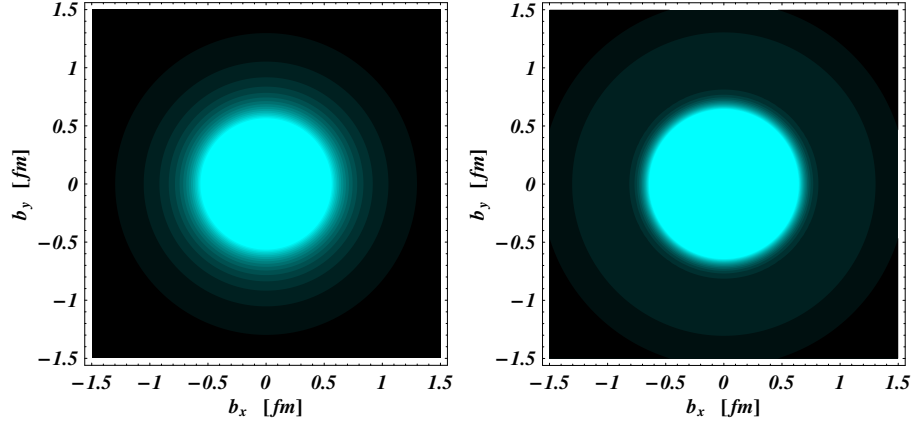


Figure 7: Quark transverse charge densities in a  $\Delta^+(1232)$  of definite light-cone helicity. Upper left panel :  $\rho_{3/2}^{\Delta}$ . Upper right panel :  $\rho_{1/2}^{\Delta}$ . The light (dark) regions correspond to the largest (smallest) values of the density. The lower panel compares the density along the  $y$ -axis for  $\rho_{3/2}^{\Delta}$  (dashed curve) and  $\rho_{1/2}^{\Delta}$  (solid curve). For the  $\Delta$  e.m. FFs, the quenched lattice QCD results are used (fit of Table 2).

In Fig. 8, the transverse densities of Eqs. (31,32) are compared for a  $\Delta^+$  that has a transverse spin. It is seen that the quark charge density in a  $\Delta^+$  in a state of transverse spin projection  $s_{\perp} = +3/2$  is elongated along the axis of the spin (prolate deformation) whereas in a state of transverse spin projection  $s_{\perp} = +1/2$  it is elongated along the axis perpendicular to the spin.



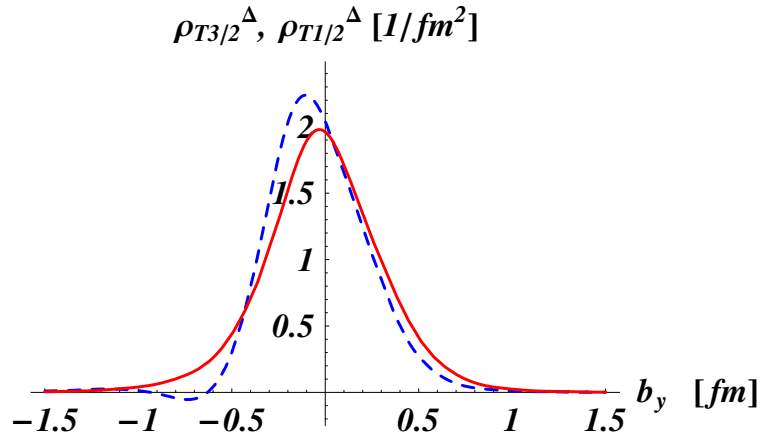
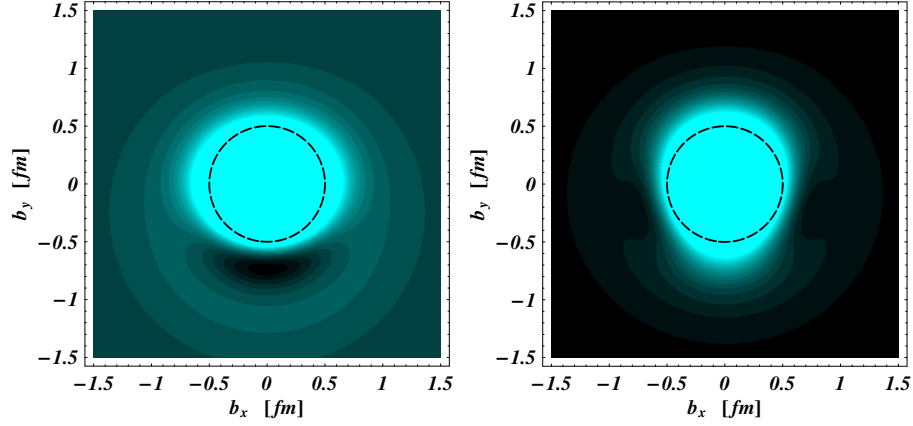


Figure 8: Quark transverse charge densities in a  $\Delta^+(1232)$  which is polarized along the positive  $x$ -axis. Upper left panel :  $\rho_{T\frac{3}{2}}^\Delta$ . Upper right panel :  $\rho_{T\frac{1}{2}}^\Delta$ . The light (dark) regions correspond to the largest (smallest) values of the density. In order to see the deformation more clearly, a circle of radius 0.5 fm is drawn for comparison. The lower panel compares the density along the  $y$ -axis for  $\rho_{T\frac{3}{2}}^\Delta$  (dashed curve) and  $\rho_{T\frac{1}{2}}^\Delta$  (solid curve). For the  $\Delta$  e.m. FFs, the quenched lattice QCD results are used (fit of Table 2).

The corresponding dipole, quadrupole and octupole field patterns in the transverse quark charge density for a transversely polarized  $\Delta$  are shown in Fig. 9.

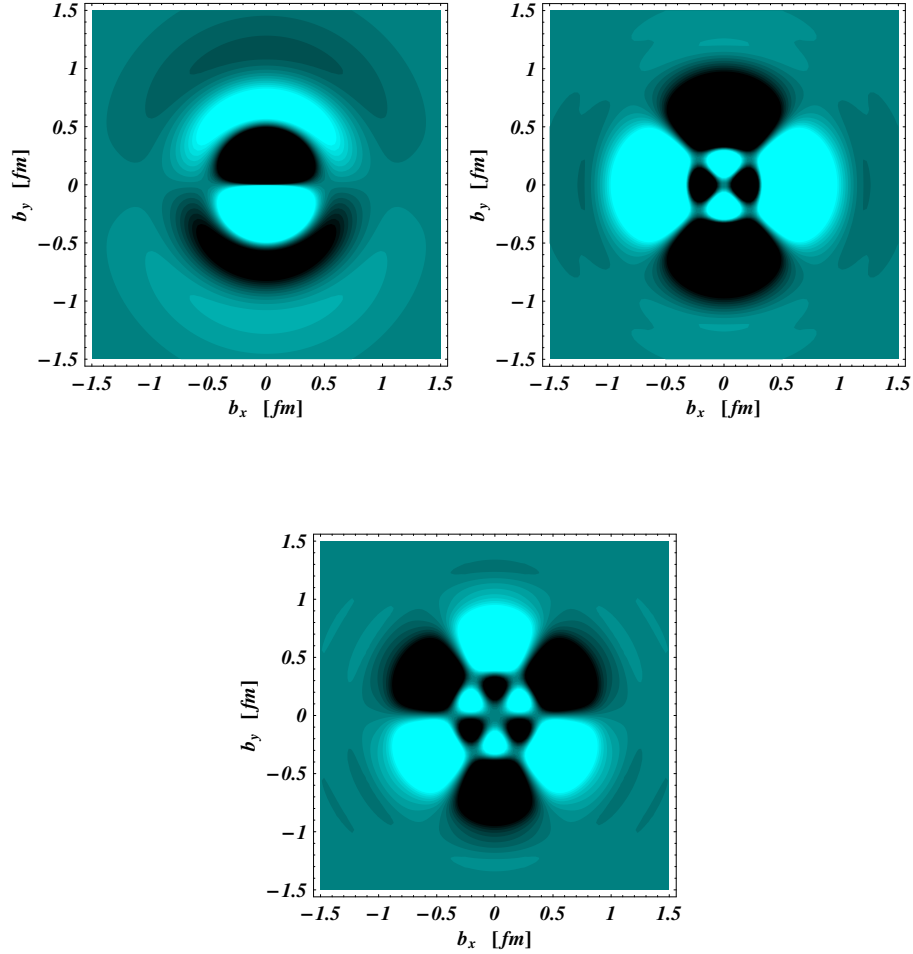


Figure 9: Multipole field patterns in the quark transverse charge density  $\rho_T^{\Delta} \frac{\Delta}{3}$  in a  $\Delta^+(1232)$  that is polarized along the positive  $x$ -axis. Upper left panel : dipole field pattern; upper right panel : quadrupole field pattern; lower panel : octupole field pattern. For the  $\Delta$  e.m. FFs, the quenched lattice QCD results are used (fit of Table 2).

To convey the consistency of all three types of simulations, we show the differences in the transverse densities between the quenched calculation and the two dynamical lattice calculations in Fig. 10. One notices that the differences are very small and arise primarily in the central densities for quenched and dynamical Wilson calculations.

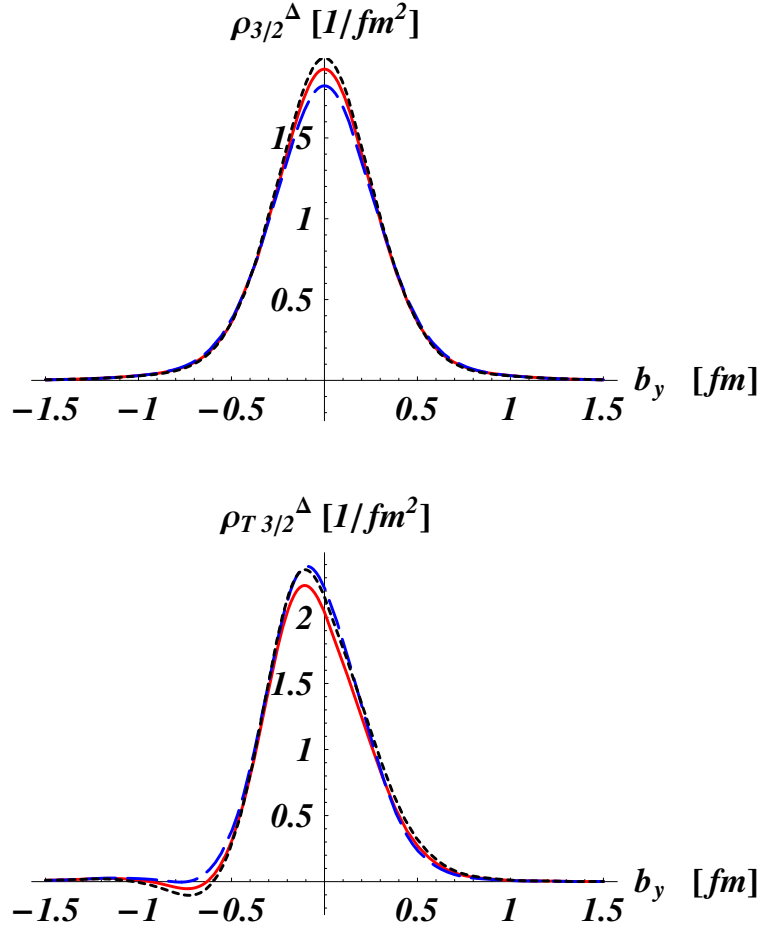


Figure 10: Comparison of the densities along the  $y$ -axis for  $\rho_{\frac{3}{2}}^{\Delta}$  (upper panel) and  $\rho_{T \frac{3}{2}}^{\Delta}$  (lower panel), for three different QCD lattice calculations of the  $\Delta^+(1232)$  e.m. FFs according to the fit of Table 2. Solid (red) curves : quenched Wilson result; long dashed (blue) curves : dynamical  $N_f = 2$  Wilson result; dotted (black) curves : hybrid lattice calculation.

## 8. Discussion and Conclusions

In this paper we have studied the electromagnetic properties of the  $\Delta(1232)$ -resonance using lattice QCD. Lattice results for the  $\Delta$  electromagnetic form factors have been presented for pion masses down to approximately 350 MeV for three cases: quenched QCD, two flavors of dynamical Wilson quarks, and three flavors of quarks described by a mixed action combining domain wall valence quarks and staggered sea quarks.

We have also presented the formalism for understanding the spin-3/2  $\Delta$  form factors in terms of precisely defined transverse quark charge density distributions in the infinite momentum, or light-front, frame. For reference, we showed that a point-like transverse charge density, that is, a two dimensional delta function, yields the specific values  $G_{E0}(0) = 1$ ,  $G_{M1}(0) = 3$ ,  $G_{E2}(0) = -3$ , and  $G_{M3}(0) = -1$  and that these values are the same as the ‘natural’ values occurring for structureless gravitinos in extended supergravity. This strongly supports the hypothesis that these are universal values characterizing structureless spin-3/2 particles. The fact that our lattice calculations yield values significantly different from these ‘natural’ values indicates the presence of interesting, nontrivial structure, and we have used the helicity amplitudes extracted from the electromagnetic form factors to construct the two-dimensional transverse quark charge densities for longitudinally and transversely polarized spins. A salient feature is that for the state with transverse spin projection 3/2, the transverse quark charge distribution is prolately deformed along the axis of the spin.

Since there is also a very different language for describing the internal deformation of the  $\Delta$  in terms of a three-dimensional intrinsic state density, it is useful to briefly summarize the status of model studies using that description and discuss the differences between the two languages. In nuclear physics, for which the nucleus is sufficiently massive that for momentum transfers characteristic of the spatial size of the nucleus, electromagnetic form factors are well described by the Fourier transform of a three-dimensional charge density, there is a fruitful history of determining the deformations of intrinsic states. The basic idea [48] is to treat collective rotations of a well-deformed nucleus in terms of a deformed intrinsic state that is axially symmetric in a body fixed-frame in which the projection of the total angular momentum  $J$  along the body-fixed symmetry axis is  $K$ . Following Ref. [48], the relation between the intrinsic quadrupole moment,  $Q_0$ , and the spectroscopic quadrupole moment,  $Q$ , measured experimentally and corresponding to the Fourier transform of the density in the lab frame, is

$$Q = \frac{3K^2 - J(J+1)}{(J+1)(2J+3)} Q_0. \quad (67)$$

In nuclear physics, this approximation is not only successful phenomenologically, but also *ab initio* nuclear mean-field theory calculations using many-body theory that accurately predict electromagnetic form factors of spherical nuclei also predict the form factors arising from deformed intrinsic states in rare-earth and actinide nuclei [49].

It is natural to ask whether this intrinsic state approximation is also applicable in studying the nucleon. One obvious example is the Skyrme model [50, 51], in which a single intrinsic soliton state generates an infinite band of collective spin-isospin rotations, with the spin-1/2 isospin-1/2 nucleon being the lowest state and the spin-3/2 isospin-3/2  $\Delta$  being the first excited state. It is clear, however, that the Skyrme model cannot be a quantitative model of the nucleon and  $\Delta$ , since the infinite tower of predicted additional states are not observed

in Nature. Buchmann and Henley [52] reviewed a variety of models of the  $\Delta$ , and concluded that for a quark model, a collective model, and a pion cloud model, the intrinsic state was oblate, corresponding to a negative value for  $Q_0$ . Studying a spheroidal bag model, Viollier, Chin, and Kerman [53] concluded that the  $K = 3/2$  intrinsic state (the same as considered by Buchmann and Henley) is oblate and that the  $K = 1/2$  intrinsic state is prolate (as in the Skyrme Model). We note that for a  $J = 3/2$   $\Delta$ , Eq. (67) specifies that for a  $K = 3/2$  intrinsic state  $Q$  and  $Q_0$  have the same sign whereas for a  $K = 1/2$  state they have opposite signs. Thus, both a prolate  $K = 1/2$  intrinsic state and oblate  $K = 3/2$  state yield a negative spectroscopic quadrupole moment, and indeed, all the results in Refs. [52, 53] are consistent with a negative value for  $Q$  and, thus by Eq. (8c), with a negative value for  $G_{E2}$  as we have calculated in Table 2. A recent calculation of the  $\Delta^+$  form factors in the chiral quark soliton model [54] found a value  $G_{E2}(0) = -2.145$ , consistent with the value of the hybrid lattice result shown in Table 2.

Unfortunately, it is not possible to go further and establish a correspondence between our result of a prolate deformation of the 2-dimensional transverse spin density along the axis of the spin-3/2 state and the model statement of an oblate intrinsic 3-dimensional density for a  $K = 3/2$  intrinsic state. As we have emphasized, even a structureless  $\Delta$  would have  $G_{E2} = -3$ , so a negative  $G_{E2}$  less negative than  $-3$  would indicate prolate deformation in our case while still being consistent with oblate deformation for an intrinsic state. It is possible that study of a simple relativistic model that could be boosted into the infinite momentum frame could go somewhat further in bridging the gap between these two different descriptions.

## Acknowledgments

It is a pleasure to acknowledge helpful discussions with Ernest Henley and Jerry Miller. This work is supported in part by the Cyprus Research Promotion Foundation (RPF) under contract ΠΕΝΕΚ/ΕΝΙΣΧ/0505-39, the EU Integrated Infrastructure Initiative Hadron Physics (I3HP) under contract RII3-CT-2004-506078 and the U.S. Department of Energy (D.O.E.) Office of Nuclear Physics under contracts DE-FG02-94ER40818 and DE-FG02-04ER41302. This research used computational resources provided by RFP under contract EPYAN/0506/08, the National Energy Research Scientific Computing Center supported by the Office of Science of the U.S. Department of Energy under Contract DE-AC03-76SF00098 and the MIT Blue Gene computer under grant DE-FG02-05ER25681. Dynamical staggered quark configurations and forward domain wall quark propagators were provided by the MILC and LHPC collaborations respectively.

## A. Lattice results for the Delta electromagnetic form factors

In Tables 3, 4, and 5, we list the lattice results for the Delta e.m. FFs in the quenched, dynamical Wilson, and hybrid calculations respectively.

	$Q^2$ (GeV <sup>2</sup> )	$G_{E0}$	$G_{M1}$	$G_{E2}$
$m_\pi = 0.563(4)$ GeV	0.173093(69)	0.7750(27)	2.340(47)	
	0.33976(26)	0.6228(41)	1.913(40)	-0.37(13)
	0.50068(54)	0.5136(54)	1.600(36)	-0.250(97)
	0.65640(89)	0.4368(68)	1.361(32)	
	0.8074(13)	0.3728(69)	1.182(29)	-0.216(72)
	0.9541(18)	0.3205(75)	1.027(29)	-0.170(60)
	1.2358(28)	0.2527(85)	0.809(31)	-0.177(57)
	1.3715(34)	0.2174(87)	0.701(31)	-0.159(50)
	1.5040(40)	0.194(10)	0.628(33)	-0.084(63)
	1.6335(46)	0.1698(97)	0.549(31)	-0.080(50)
	1.7603(53)	0.142(11)	0.460(38)	-0.136(57)
	1.8845(59)	0.140(12)	0.439(35)	-0.100(55)
	2.0063(66)	0.117(10)	0.372(31)	-0.085(44)
2.2430(79)	0.084(16)	0.284(47)		
$m_\pi = 0.490(4)$ GeV	0.172859(82)	0.7646(32)	2.324(58)	
	0.33890(30)	0.6076(46)	1.889(48)	-0.41(16)
	0.49887(64)	0.4965(61)	1.575(43)	-0.27(12)
	0.6534(11)	0.4212(77)	1.329(37)	
	0.8030(15)	0.3574(75)	1.155(34)	-0.209(85)
	0.9481(21)	0.3055(83)	1.004(33)	-0.160(70)
	1.2263(33)	0.2428(90)	0.797(35)	-0.196(68)
	1.3600(40)	0.2060(93)	0.682(35)	-0.167(61)
	1.4906(47)	0.182(11)	0.608(37)	-0.054(76)
	1.6181(54)	0.159(10)	0.531(34)	-0.062(59)
	1.7427(61)	0.131(12)	0.440(41)	-0.151(72)
	1.8648(68)	0.133(12)	0.432(39)	-0.118(65)
	1.9844(76)	0.110(10)	0.358(33)	-0.091(50)
2.2167(91)	0.073(16)	0.259(47)		
$m_\pi = 0.311(4)$ GeV	0.172616(98)	0.7546(42)	2.320(78)	
	0.33800(36)	0.5933(55)	1.876(62)	-0.50(22)
	0.49700(75)	0.4797(72)	1.558(54)	-0.32(15)
	0.6503(12)	0.4061(92)	1.295(48)	
	0.7985(18)	0.3422(84)	1.131(41)	-0.20(12)
	0.9420(24)	0.2908(95)	0.987(41)	-0.170(87)
	1.2167(39)	0.236(10)	0.797(41)	-0.244(90)
	1.3485(46)	0.196(10)	0.665(41)	-0.199(83)
	1.4770(54)	0.172(12)	0.590(43)	-0.03(10)
	1.6025(62)	0.150(11)	0.518(39)	-0.041(79)
	1.7250(70)	0.121(13)	0.417(48)	-0.19(11)
	1.8450(79)	0.127(13)	0.436(46)	-0.193(88)
	1.9624(87)	0.103(11)	0.349(37)	-0.117(62)
2.190(10)	0.066(17)	0.231(52)		

Table 3: Delta form factors from quenched Wilson fermions.

	$Q^2$ (GeV $^2$ )	$G_{E0}$	$G_{M1}$	$G_{E2}$
$m_\pi = 0.691(8)$ GeV	0.43260(36)	0.6248(40)	1.900(50)	
	0.8364(13)	0.4352(65)	1.348(44)	-0.33(15)
	1.2164(25)	0.337(11)	0.998(49)	-0.17(12)
	1.5765(40)	0.282(19)	0.761(56)	
	1.9195(56)	0.235(22)	0.638(58)	-0.12(10)
	2.2475(74)	0.189(21)	0.501(61)	-0.095(79)
	2.866(11)	0.125(32)	0.312(84)	-0.012(96)
	3.159(13)	0.103(24)	0.225(56)	-0.043(75)
	3.442(15)	0.069(19)	0.136(43)	-0.155(96)
	3.717(17)	0.054(27)	0.129(58)	-0.04(11)
	3.984(19)	0.081(47)	0.106(70)	-0.12(18)
	4.244(21)	0.034(13)	0.087(32)	-0.008(58)
	4.497(23)	0.040(33)	0.078(72)	-0.010(93)
	4.985(27)	0.019(34)	-0.004(49)	
$m_\pi = 0.509(8)$ GeV	0.42932(57)	0.5748(85)	1.743(76)	
	0.8250(20)	0.3785(82)	1.199(55)	-0.49(21)
	1.1939(39)	0.288(13)	0.745(60)	-0.41(19)
	1.5409(61)	0.241(30)	0.546(78)	
	1.8694(85)	0.181(16)	0.433(55)	-0.15(12)
	2.182(11)	0.194(51)	0.36(11)	-0.04(13)
	2.768(16)	0.093(33)	0.181(75)	-0.22(14)
	3.044(19)	0.037(18)	0.043(37)	0.004(91)
	3.311(22)	0.019(15)	0.039(26)	-0.021(84)
	3.569(25)	0.021(39)	0.032(62)	-0.06(14)
	3.819(27)	0.045(41)	-0.009(59)	0.05(17)
	4.062(30)	0.013(16)	0.020(29)	-0.018(74)
	4.298(33)	0.003(19)	-0.001(27)	0.099(82)
	4.753(38)	0.015(43)	-0.00(11)	
$m_\pi = 0.384(8)$ GeV	0.42485(79)	0.566(15)	1.530(92)	
	0.8099(26)	0.368(16)	1.048(62)	-0.53(27)
	1.1647(50)	0.276(32)	0.891(97)	-0.41(24)
	1.4953(77)	0.195(48)	0.57(11)	
	1.806(11)	0.141(80)	0.354(39)	-0.30(15)
	2.100(14)	0.11(12)	0.337(61)	-0.27(15)
	2.648(20)	0.11(25)	0.062(99)	-0.42(49)
	2.905(23)	0.05(31)	0.095(37)	0.04(12)
	3.152(26)	0.04(39)	0.084(53)	-0.48(24)
	3.391(29)	0.03(47)	0.047(95)	-0.19(39)
	3.622(32)	0.04(57)	-0.040(94)	0.17(23)
	3.846(35)	0.03(68)	0.001(54)	-0.05(20)
	4.063(38)	0.04(78)	0.014(35)	-0.06(10)
	4.481(44)	-0.0(1.0)	0.011(69)	

Table 4: Delta form factors from dynamical Wilson fermions.

	$Q^2$ (GeV <sup>2</sup> )	$G_{E0}$	$G_{M1}$	$G_{E2}$
$m_\pi = 0.353(2)$ GeV	0.124094(51)	0.8223(95)	2.83(21)	
	0.24512(19)	0.686(13)	2.26(17)	-1.47(88)
	0.36330(42)	0.584(17)	1.99(17)	-0.84(72)
	0.47881(71)	0.499(22)	1.89(17)	
	0.5918(11)	0.432(21)	1.53(14)	-0.76(48)
	0.7025(15)	0.386(23)	1.38(14)	-0.56(46)
	0.9175(24)	0.310(29)	1.15(14)	-0.20(44)
	1.0220(29)	0.287(35)	1.04(15)	-0.47(43)
	1.1246(35)	0.239(31)	0.83(13)	-0.05(47)
	1.2255(41)	0.223(34)	0.78(14)	-0.44(47)
	1.3247(47)	0.261(88)	0.90(31)	-0.72(65)
	1.4223(53)	0.187(35)	0.67(12)	-0.38(43)
	1.5184(59)	0.176(45)	0.65(16)	-0.81(48)
	1.7064(73)	0.094(42)	0.27(15)	
	1.7983(80)	0.125(45)	0.41(13)	-0.64(48)
	1.8890(87)	0.095(34)	0.327(85)	-0.40(39)
	1.9785(94)	0.101(40)	0.30(13)	-0.84(64)
	2.067(10)	0.073(35)	0.276(87)	-0.39(44)
	2.154(11)	0.073(37)	0.191(84)	-0.51(43)
	2.240(12)	0.124(89)	0.23(27)	-1.3(1.4)
2.409(13)	0.079(55)	0.16(16)	-0.45(71)	

Table 5: Delta form factors from the hybrid approach.

## References

- [1] C. E. Hyde-Wright and K. de Jager, *Ann. Rev. Nucl. Part. Sci.* **54**, 217 (2004).
- [2] J. Arrington, C. D. Roberts and J. M. Zanotti, *J. Phys. G* **34**, S23 (2007).
- [3] C. F. Perdrisat, V. Punjabi and M. Vanderhaeghen, *Prog. Part. Nucl. Phys.* **59**, 694 (2007).
- [4] M. Burkardt, *Phys. Rev. D* **62**, 071503 (2000) [Erratum-ibid. *D* **66**, 119903 (2002)] [arXiv:hep-ph/0005108].
- [5] G. A. Miller, *Phys. Rev. Lett.* **99**, 112001 (2007).
- [6] C. E. Carlson and M. Vanderhaeghen, *Phys. Rev. Lett.* **100**, 032004 (2008).
- [7] C. E. Carlson and M. Vanderhaeghen, arXiv:0807.4537 [hep-ph].
- [8] G. A. Miller, arXiv:0901.1117 [nucl-th].
- [9] V. Pascalutsa, M. Vanderhaeghen and S. N. Yang, *Phys. Rept.* **437**, 125 (2007).
- [10] C. Alexandrou, G. Koutsou, H. Neff, J. W. Negele, W. Schroers and A. Tsapalis, *Phys. Rev. D* **77**, 085012 (2008).



- [11] C. Alexandrou *et al.*, arXiv:0810.3976 [hep-lat].
- [12] S. Nozawa and D. B. Leinweber, Phys. Rev. D **42**, 3567 (1990).
- [13] H. J. Weber and H. Arenhovel, Phys. Rept. **36**, 277 (1978).
- [14] D. B. Leinweber, T. Draper and R. M. Woloshyn, Phys. Rev. D **46**, 3067 (1992).
- [15] C. Amsler *et al.* [Particle Data Group], Phys. Lett. B **667**, 1 (2008).
- [16] M. Kotulla *et al.*, Phys. Rev. Lett. **89**, 272001 (2002).
- [17] D. Drechsel and M. Vanderhaeghen, Phys. Rev. C **64**, 065202 (2001).
- [18] M. Kotulla, in Proceedings of the 11th Workshop on “The Physics of Excited Nucleons” (NSTAR2007). Eds. H.-W. Hammer, V. Kleber, U. Thoma, and H. Schmieden.
- [19] L. Tiator, D. Drechsel, S. S. Kamalov and S. N. Yang, Eur. Phys. J. A **17**, 357 (2003).
- [20] A. J. Buchmann, J. A. Hester and R. F. Lebed, Phys. Rev. D **66**, 056002 (2002).
- [21] S. Weinberg in “Lectures on Elementary Particles and Quantum Field Theory”, Volume 1, Brandeis University Summer Institute 1970 (S. Deser, M. Grisaru and H. Pendleton, editors, M.I.T. Press, Cambridge, 1970).
- [22] S. Ferrara, M. Porrati and V. L. Telegdi, Phys. Rev. D **46**, 3529 (1992).
- [23] B. R. Holstein, Am. J. Phys. **74**, 1104 (2006).
- [24] S. Ferrara and P. van Nieuwenhuizen, Phys. Rev. Lett. **37**, 1669 (1976).
- [25] P. Van Nieuwenhuizen, Phys. Rept. **68**, 189 (1981).
- [26] S. Deser, V. Pascalutsa and A. Waldron, Phys. Rev. D **62**, 105031 (2000).
- [27] K. Johnson and E. C. Sudarshan, Annals Phys. **13**, 126 (1961)
- [28] G. Velo and D. Zwanziger, Phys. Rev. **186**, 1337 (1969).
- [29] C. Alexandrou, T. Korzec, T. Leontiou, J. W. Negele and A. Tsapalis, PoS **LAT2007**, 149 (2007).
- [30] C. Aubin, K. Orginos, V. Pascalutsa and M. Vanderhaeghen, arXiv:0811.2440 [hep-lat].
- [31] C. W. Bernard *et al.*, Phys. Rev. D **64**, 054506 (2001).
- [32] D. B. Renner *et al.* [LHP Collaboration], Nucl. Phys. Proc. Suppl. **140**, 255 (2005).

- [33] Ph. Hagler *et al.* [LHPC Collaborations], Phys. Rev. D **77**, 094502 (2008).
- [34] J. W. Chen, D. O'Connell and A. Walker-Loud, arXiv:0706.0035 [hep-lat].
- [35] C. Alexandrou *et al.* [European Twisted Mass Collaboration], Phys. Rev. D **78**, 014509 (2008).
- [36] C. Alexandrou, S. Gusken, F. Jegerlehner, K. Schilling and R. Sommer, Nucl. Phys. B **414**, 815 (1994).
- [37] Montvay, I. and Münster, G., *Quantum Fields on a Lattice*, Cambridge University Press, 1994.
- [38] D. Dolgov *et al.* [LHPC collaboration and TXL Collaboration], Phys. Rev. D **66**, 034506 (2002).
- [39] B. Orth, T. Lippert and K. Schilling, Phys. Rev. D **72**, 014503 (2005).
- [40] C. Urbach, K. Jansen, A. Shindler and U. Wenger, Comput. Phys. Commun. **174**, 87 (2006).
- [41] C. Alexandrou, G. Koutsou, J. W. Negele and A. Tsapalis, Phys. Rev. D **74**, 034508 (2006).
- [42] R. Sommer, Nucl. Phys. B **411**, 839 (1994).
- [43] C. Aubin *et al.*, Phys. Rev. D **70**, 094505 (2004).
- [44] C. Michael and J. Peisa (UKQCD), Phys. Rev. **D58** 034506 (1998); C. Michael and J. Peisa [UKQCD Collaboration], Nucl. Phys. Proc. Suppl. **60A**, 55 (1998).
- [45] J. Foley *et al.*, Comput. Phys. Commun. **172**, 145 (2005); C. Alexandrou, P. Dimopoulos, G. Koutsou and H. Neff, PoS **LAT2005**, 030 (2006); C. Alexandrou, G. Koutsou and H. Neff, PoS **LAT2006**, 113 (2006); C. Alexandrou and G. Koutsou, PoS **LAT2007**, 150 (2007); S. Collins, G. Bali and A. Schafer, PoS **LAT2007** 141 (2007); C. Alexandrou and G. Koutsou, Phys. Rev. (2008), arXiv:0809.2056;
- [46] K. Jansen, C. Michael and C. Urbach (ETM Collaboration), arXiv:0804.3871 (2008).
- [47] W. Wilcox, Walter, Nucl. Phys. Proc. Suppl. **94**, 319 (2001), hep-lat/0010060.
- [48] A. Bohr and B. Mottelson, *Nuclear Structure II* Benjamin, Reading, MA, (1975).
- [49] J. W. Negele and G. Rinker, Phys. Rev. C **15**, 1499 (1977).
- [50] T. H. R. Skyrme, Proc. Roy. Soc. Lond. A **260**, 127 (1961).

- [51] T. H. R. Skyrme, Nucl. Phys. **31**, 556 (1962).
- [52] A. J. Buchmann and E. M. Henley, Phys. Rev. C **63**, 015202 (2001) [arXiv:hep-ph/0101027].
- [53] R. D. Viollier, S. A. Chin and A. K. Kerman, Nucl. Phys. A **407**, 269 (1983).
- [54] T. Ledwig, A. Silva and M. Vanderhaeghen, arXiv:0811.3086 [hep-ph].